UNIVERSITEIT VAN PRETORIA
UNIVERSITY OF PRETORIA
YUNIBESITHI YA PRETORIA

Analysis of the role of nuclear factor-kappa B in insulin resistance caused by antiretroviral drugs

By

Matamela Charles Mabugana

13077695

Supervisor: Prof Tahir S. Pillay[1]

[1]Department of Chemical Pathology, University of Pretoria, South Africa

Submitted in partial fulfilment of the requirements of the degree of

MSc Chemical Pathology

Faculty of Health Sciences

University of Pretoria

Pretoria

December 2020

Declaration

I, Matamela Charles Mabugana, declare that the thesis/dissertation, which I hereby submit for the degree MSc Chemical Pathology at the University of Pretoria, is my own work and has not previously been submitted by me for a degree at this or any other tertiary institution.

SIGNATURE: 

DATE: 10 /12/2020

Contents

List of Figures

List of Tables

Acknowledgements

First and foremost, I would like to thank the Good Lord of Mount Zion for the blessings, knowledge, wisdom and strength to carry out this research. Philippians 4:13 " I can do all this through Him who gives me strength". I would like to extend my gratitude to the National Research Foundation (NRF) for funding my project. To my supervisor, Prof Tahir Pillay, I will forever be grateful for your support and guidance. Thank you for all your hard work in the project and your motivation.

I am grateful to my parents Mashudu and Johannes Mabugana, ndi livhuwa thikhedzo na thuthuwedzo yavho. My siblings and niblings, thank you for always being there for me in this period. To Dr Chale-Matsau, thank you for your emotional support, I will forever be grateful for that. Mr Mathomu, Dr Iman van den Bout and Mr Mabate thank you for providing me with antibodies, competent cells and for proofreading this, respectively. Microbiology department (University of Pretoria) for allowing me to use some of their facilities for some of my experiments. The STIRC family, you have always been a cornerstone.

To all my friends, Gcino, Howard, Takalani, Arinao , Uarine and Kgaogelo, thanks for playing an integral part during this time. Inspired by Snoop Dogg, last but not least, I want thank me, for believing in me, for doing all this hard work, for having no days off, for never quitting even when it seems to be the way out. 1 Thessalonians 5:16-18 "Rejoice always, pray continually, give thanks in all circumstances; for this is God's will for you in Christ Jesus"

Abstract

Human immunodeficiency virus still remains the leading cause of death globally including women of child-bearing age. The rate of AIDS related death have significantly decline since the introduction of the antiretroviral treatment and other non-medical interventions such as the distribution and use of condoms. The introduction of antiretroviral treatment has however led to insulin resistance amongst users. Clustered regularly interspaced short palindromic repeats (CRISPR) CRISPR-associated nuclease 9 (Cas) has been used to knockout NFκB to understand the pathway at which antiretroviral treatment cause insulin resistance. Heteroduplex mobility assay has shown that CRISPR-Cas9 knockout the gene of interest. These results has layed a foundation in understanding how CRISPR-Cas9 can be integrated and utilised in medical research.

Keyword: CRISPR-Cas9, insulin resistance, HAART, NFκB,

List of abbreviations

ACC	acetyl coenzyme-A carboxylase
AGE	advanced glycation end products
AMPK	AMP-activated protein kinase
Ang II	angiotensin II
aPKC	acute protein kinase C
APS	adaptor protein with pleckstrin homolohy and Src homology 2 domain
ARV	antiretrovirals
ATM	ataxia telangiectasia mutated-
ATP	adenosine triphosphate
BAFFR	B-cell activated factor receptor
Cas9	CRISPR associated protein 9
CCR5	chemokine receptor 5
CD4	cluster of differentiation
cDNA	complementary DNA
CHO-IR	Chinese hamster ovarian cell transfected with insulin receptors
CIS	cytosine-induced STAT inhibitor
cPKC	conventional protein kinase C
CREBH	cAMP-response element-binding protein H
CRISPR	clustered regularly interspaced short palindromic repeats
crRNA	CRISPR RNA
DAG	diacylglycerol
ddH_2O	double distilled water
DNA	deoxyribose nucleic acid
ER	endoplasmic reticulum
ETC	electron transport chain
FFA	free fatty acid

GLUT4	glucose transporter type 4
gRNA	guide RNA
HAART	highly active antiretroviral therapy
HDR	homologous directed repair
HIV	Human Immunodeficiency Virus
IKK	inhibitor of NFκB kinase
IKK-β	inhibitor of NFκB kinase β
IL6	interleukin 6
InSTI	integrase strand transfer inhibitor
IRS	insulin receptor substrate
IκB	inhibitor of kappa B
JNK	c-Jun N-terminal kinase
LTβR	lymphotoxin β-receptor
NAFLD	non-alcoholic fatty liver disease
NEFA	nonesterified fatty acids
NEMO	NFκB essential modulator
NFκB	nuclear factor kappa B
NHEJ	non-homologous end-joining
NIK	NFκB-induced kinase
NLS	nuclear localisation sequence
NNRTI	non-nuclease reverse transcriptase inhibitor
nPKC	novel protein kinase C
NRTI	nuclease reverse transcriptase inhibitor
ORF	open reading frame
PCR	polymerase chain reaction
PDK	PIP_3 – dependant protein kinase
PEPCK	phosphoenolpyruvate carboxykinase
PH	pleckstrin homology
PI	protease inhibitor

PI3K	phosphoinositide 3-kinase
PIP_2	phosphatidylinositol 4,5-biphosphate
PIP_3	phosphatidylinositol 3,4,5-triphosphate
PKC	protein kinase C
PPARγ	proliferator-activated receptor gamma
RAGE	receptors for AGE
RNS	reactive nitrogen species
ROS	reactive oxygen species
RVD	repeat-variable di-residues
SCD	stearoyl-CoA desaturates
SCID	Severe Combined Immune Deficiency
SH_2B	Src homology 2B
SOCS	suppressor of cytokine signal
SREBP-1	sterol regulatory element binding protein sub-type 1
STATS-SA	Statistics South Africa
TALEN	transcription activator-like effector nuclease
TLR-4	Toll-like receptor 4
TNF	tumour necrosis factor
TNFR	tumour necrosis factor receptor
tracrRNA	trans-activating RNA
VLDL	very low-density lipoprotein
WHO	World Health Organisation
ZFN	zinc-finger nuclease

List of Symbols

κ	kappa
μ	micro
α	alpha
∞	undefined
°	degree

Chapter 1

1.1. Introduction

Since the early 80's when HIV was first discovered, there has been no cure developed. However, there are combinations of drugs that are used to manage the infection and improve life expectancy. These drugs are inclusive of nuclease analogue reverse transcriptase inhibitors (NRTIs), non-nucleoside reverse transcriptase inhibitors (NNRTIs), protease inhibitors (PI) and fusion inhibitors (Arts and Hazuda, 2012). Despite the improved life expectancy, these drugs have multiple side effects. These include the induction of insulin resistance, which leads to diabetes mellitus, dyslipidemia, lipodystrophy, and inflammation depending to class of drugs (Arts and Hazuda, 2012).

Diabetes mellitus is a clinical disease that occurs as results of insulin deficiency or insulin resistance. Insulin deficiency arises when the pancreatic beta cells undergo apoptosis and autoimmune-induced inflammation. This condition is referred to as type I diabetes mellitus. On the other hand, Type 2 diabetes mellitus is caused by insulin resistance and is characterised by visceral adipose tissue and obesity (Akash *et al.,* 2017). Adipose tissue plays a crucial role in insulin action as it secretes adipokines that regulate insulin action and, it is also a significant target tissue for the effects of insulin.

Insulin resistance is a state where there is a compromised biological response to insulin in the presence of either standard or elevated insulin levels. Insulin resistance arises from various factors such as obesity where there are impaired insulin responses and increased inflammatory signaling that regulates proteins in the insulin receptor signaling pathway (Hoesel and Schmid, 2013). Typically, the elevation of tumour necrosis factor (TNF) or high-levels of free fatty acids induces inhibitory serine phosphorylation of IRS-1, thus interrupting the insulin signal transduction and as a consequence leading to insulin resistance. c-Jun N-terminal kinase (JNK), an inhibitor of nuclear factor (NF)-κB kinase (IKK) and protein kinase C (PKC) are examples of the serine/threonine kinases whose activation either by stress or inflammation contributes the inhibition of insulin signaling (Perkins and Gilmore, 2006). The activation of NF-κB and the activator protein (AP)-1 complexes can induce further inflammatory gene expression due to these kinases. Also, in a previous study, the NF-κB pathway was implicated in the insulin resistance induced by protease inhibitors (Ismail *et al.,* 2013) in the CHO-IR cell line.

This study intended to explore the mechanisms by which antiretroviral drugs induced insulin resistance. To further elucidate the role of the NF-κB pathway, the NF-κB gene was deleted in the Chinese Hamster Ovarian cell transfected with insulin receptors (CHO-IR) cell line in an attempt to determine the effect of antiretroviral drugs on NF-κB downstream protein.

1.2. Human immunodeficiency virus

Human immunodeficiency virus (HIV) is categorised in genus Lentivirus in Retroviridae family and Orthoretrovirinae subfamily (Luwic, 1996). The common types known are HIV-1 and HIV-2, where their classification depends on the genetic characteristics of the viral antigen (Luwic, 1996). It is reported that HIV-1 evolved from non-human primates, a Central African chimpanzees immunodeficiency virus (SIV cpz) and HIV-2 evolving from West African sooty mangabeys (SIVsm) (Gao *et al.,*1999; Utech and Berneis, 2005).

Although it is manageable and has been transformed from fatal disease to a chronic illness, prolonging HIV patients' lives, HIV is still a burden (Aboud *et al.,* 2007, Utech and Berneis, 2005). According to the world health organisation (WHO) report of 2017, more than 35 million people have died from HIV since its discovery, and about 940 000 of those died in 2017 alone. From the same report, 36.9 million people are living with the disease, with new infections of 1.8 million per annum globally. From the total infection, two-thirds equating to 25.7 million, of those are reported in an African region making it the most infected region. Of total infected persons, about 59 % of adults and 52 % of youth are receiving ARVs as of 2017 (WHO, 2017).

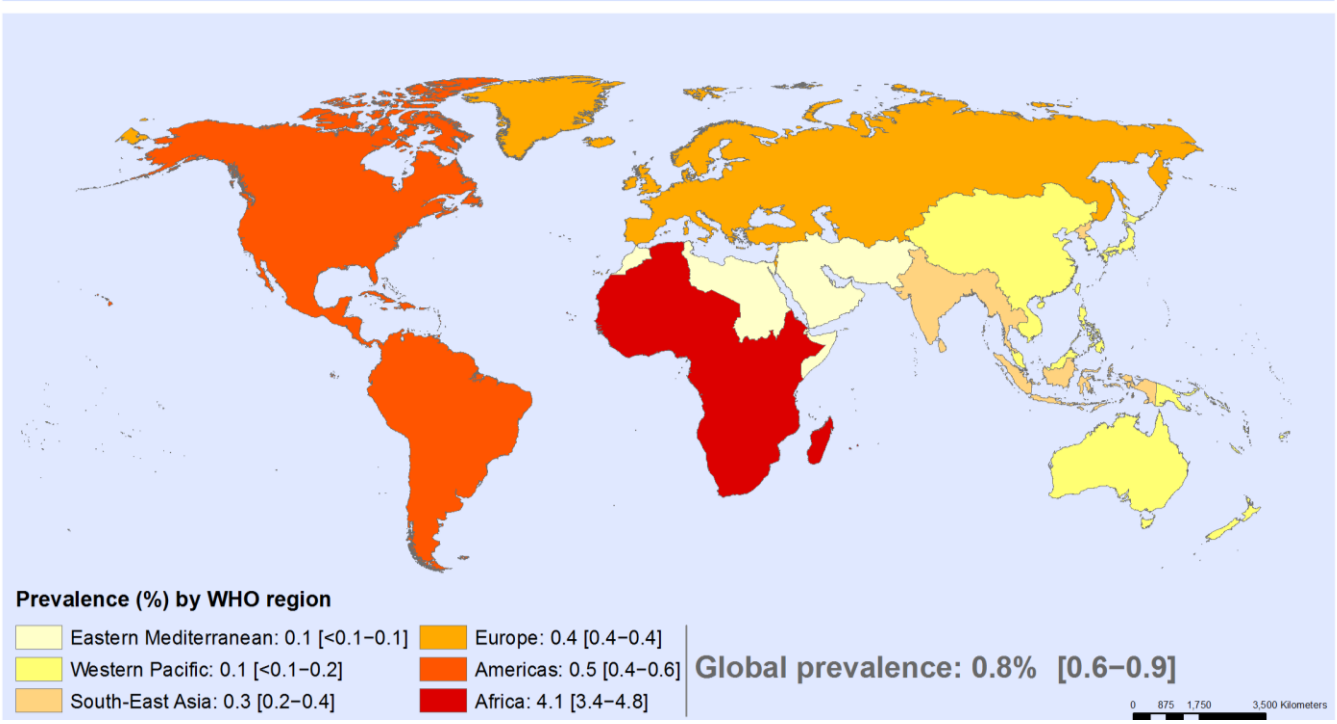

Figure 1.1. The prevalence of HIV in adults aged 15 to 49 in 2017 around the globe *(WHO 2018).*

In South Africa, in 2018, 7.52 million people were living with the disease, a 3.27 million increase from an estimated 4.25 million in 2002 (STATS SA, 2018). The STATS SA estimated that about 13.1 % of the total South African population is HIV positive (STATS SA, 2018). According to UNAIDS Data of 2017, there were 270 000 new infections in 2016. About 56 % of adults and 55 % of children were on ARV treatment in 2016 (UNAIDS, 2017).

1.2.1. HIV morphology

A typical HIV particle has a round shape, enclosed by a lipid envelop with 72 knobs and is approximately 100 nm in diameter (Gelderblom, 1991). An HIV particle comprises of two identical single-stranded RNA molecules enclosed in the core of the virus (Eberle and Gurtler, 2012). The HIV provirus genomic DNA is generated by reverse transcription of the viral RNA, degrading RNA and integration into the human genome. The DNA has long terminal repeat (LTR) sequences at both ends, whereby the 5'LTR codes for a promoter for transcription of the viral gene (Eberle and Gurtler, 2012).

Various genes are crucial for viral make-up. These genes include the *gag* responsible for the outer core membrane and capsid protein, *pol* coding for protease enzymes, reverse transcriptase, RNase H and integrase. Adjacent to *pol* gene lies *env,* which is responsible for envelope glycoproteins. Besides the structural proteins, HIV also codes for regulatory proteins, which includes *tat* and *rev* responsible for HIV replication initiation; *nef, vif, vrp,* and *vpu* responsible for viral replication, budding and pathogenesis (Seitz, 2016; Eberle and Gurtler, 2012).

1.2.2. HIV life cycle and pathogenesis

The protein-protein interaction between surface glycoprotein of mature HIV and CD4 receptors on the host cell, which includes T helper cell, macrophages, dendritic cells, and astrocytes initiates the life cycle and pathogenesis. After attachment follows a conformational change in CD4 cells, opening additional sites for glycoprotein binding, including chemokine receptor 5 (CCR5) (Dean *et al.,* 1996). The glycoprotein, due to its high hydrophobicity characteristic, leads to translocation of viral capsid into the host's cytoplasm (Eberle and Gurtler, 2012). The viral capsid is then taken up by an endosome, where it releases its contents stimulated by the pH change (Stein *et al.,* 1987). In the cytoplasm, reverse transcriptase is activated.

Reverse transcriptase transcribes the single-stranded HIV DNA genome into complementary DNA (cDNA) (Eberle and Gurtler,2012). Simultaneously, RNA is degraded by RNase H. The single-stranded cDNA is then converted to a double-stranded proviral DNA by DNA-dependent DNA polymerase activity of reverse transcriptase (Sousa *et al.,* 1993). The newly synthesised DNA is transported into the nucleus via nucleopores to form complexes with integrase which inserts it into the host's cell genome. The viral genome is replicated together with the host cell genome during cell division (Sousa *et al.,* 1993). The host's transcription machinery transcribes HIV DNA into multiple copies of new HIV RNA. Some of those rna becomes viral genome while others are used by cells to make viral protein. The newly transcribed RNA and proteins move to the surface of the cell. Here, a new immature HIV virus are formed. The viruses are then released from the cell. Protease cleaves newly synthesised polyproteins to create infectious virus (Sousa *et al.,* 1993).

1.3. Highly active antiretroviral therapy

Highly active antiretroviral therapy (HAART) is a combination of three or more antiretroviral (ARV) agents for the treatment of HIV infection (Aboud *et al.,* 2007; Matthews *et al.,* 2004). Since its discovery in the mid-1990s, it showed an immediate benefit. There was a transformation of HIV categorisation from a fatal disease to a chronic disease, prolonging HIV patients' lives (Abound *et al.,* 2007; Matthews *et al.,* 2004). Between the year 2000 and 2017, HIV-related death fell by 36 % and about 11.4 million lives saved due to ARVs (WHO, 2017). Drugs currently in use are summarised in table 1.1 below.

Table 1.1 Categories of ARVs according to the mode of action, their generic names and product names.

Antiviral drug class	Generic name	Product name (supplier)
Nucleoside/nucleotide reverse transcriptase inhibitor	Abacir	Ziagen (GlaxoSmithKline)
	Didanosine	Videx (Bristol-Myers Squibb)
	Lamivudine	Epivir (GlaxoSmithKline)
	Stavudine	Zerit (Bristol-Myers Squibb)
	Zidovudine	Retrovir (GlaxoSmithKline)
	Zidovudine/lamivudine	Combivir (GlaxoSmithKline)
Non-nucleoside reverse transcriptase inhibitor	Efavirenz	Sustiva (Bristol-Myers Squibb)
	Nevirapine	Viramune (Boehringer Ingelheim)
Protease inhibitors	Indinavir	Crixivan (Merk)
	Ritonavir	Norvir (Abbott Laboratories)
	Saquinavir	Invirase (Roche)
	Lopinavir/ritonavir	Kaletra (Abbott Laboratories)
Fusion inhibitor	Enfuvirtide	Fuzeon (Hoffmann-La Roche inc)

Combination of antiretroviral therapy achieved the dramatic benefits by suppressing viral replication and reduce viral load in plasma. This was measured by the increase in the circulation of $CD4^+$ (Arts and Hazuda, 2012). The use of three or more drugs at once have advantages as it decreases the probability of new strain formation due to mutation (Arts and Hazuda, 2012). Currently, six classes of these drugs have been established based on their mechanism of action. They are nucleoside/nucleotide reverse transcriptase inhibitors (NRTI), non-nucleoside reverse transcriptase inhibitors (NNRTI), integrase inhibitors, protease inhibitors (PI), fusion inhibitors and co-receptor antagonists (Arts and Hazuda, 2012; Neuman, *et al.,* 2009). The modes of action of all HAART classes are explained below.

i. Nucleoside/nucleotide reverse transcriptase inhibitors

Typically, NRTIs are administered as pro-drugs and thus require entrance into the host cell and trigger cellular kinases phosphorylation (Aposolova *et al*., 2011). NRTIs are competitive inhibitors of reverse transcriptase enzyme-substrate lacking a 3'-hydroxyl group in their sugar. This prevents 3'-5' bond between NRTI and incoming 5'-nucleoside triphosphates leading into the termination of DNA chain growth (Arts and Hazuda, 2012; Apostolova *et al*., 2011).

ii. Non-nucleoside reverse transcriptase inhibitors

The NNRTIs are non-competitive inhibitors that act as inhibitors of HIV-1 reverse transcriptase by attaching and forming a hydrophobic pocket proximal to an active site (Tantillo *et al.,* 1994).

This binding reduces the polymerase activity by changing the spatial conformation of the substrate-binding site (Kohlstaedt *et al.,* 1992). Unlike NRTIs, NNRTIs cannot inhibit the reverse transcriptase of other lentiviruses, including HIV-2 isoform (Kohlstaedt *et al.,* 1992).

iii. Integrase inhibitors

In HIV life cycle, integrase plays a crucial role by catalysing the 3' end processing together with viral DNA and strand transfer. Integrase inhibitors are synthesised to retard the strand transfer reaction. Thus, sometimes are referred to as integrase strand transfers inhibitor (InSTI) (Hazuda *et al.,* 2004). The inhibitor binding achieves a specific complex between integrase' and the viral DNA. The inhibitor also interacts with magnesium metal ion cofactors in the integrase active site. Thus, InSTI are made of metal-binding pharmacophore and a hydrophobic that typically interacts with viral DNA (Grobler *et al.,* 2002).

iv. Fusion inhibitors

Fusion inhibitors are types of inhibitors that inhibit viral entry. It is a homolog to heptad-repeat 2(HR2) and 36 amino acid long. It binds to heptad-repeat 1 (HR1) motif and inhibits the formation of a six-helix bundle required for fusion (Lalezari *et al.,* 2003). The HR-1 and -2 are 41 gp motifs that unite to form a six-helix bundle hairpin structure, which pulls the membrane of the virus and cell closer to fuse the membrane (Lalezari *et al.,* 2003). This cause blockage of viral particle from gaining access to the cell. Figure 1.2 below summarizes mode of action of HAART.

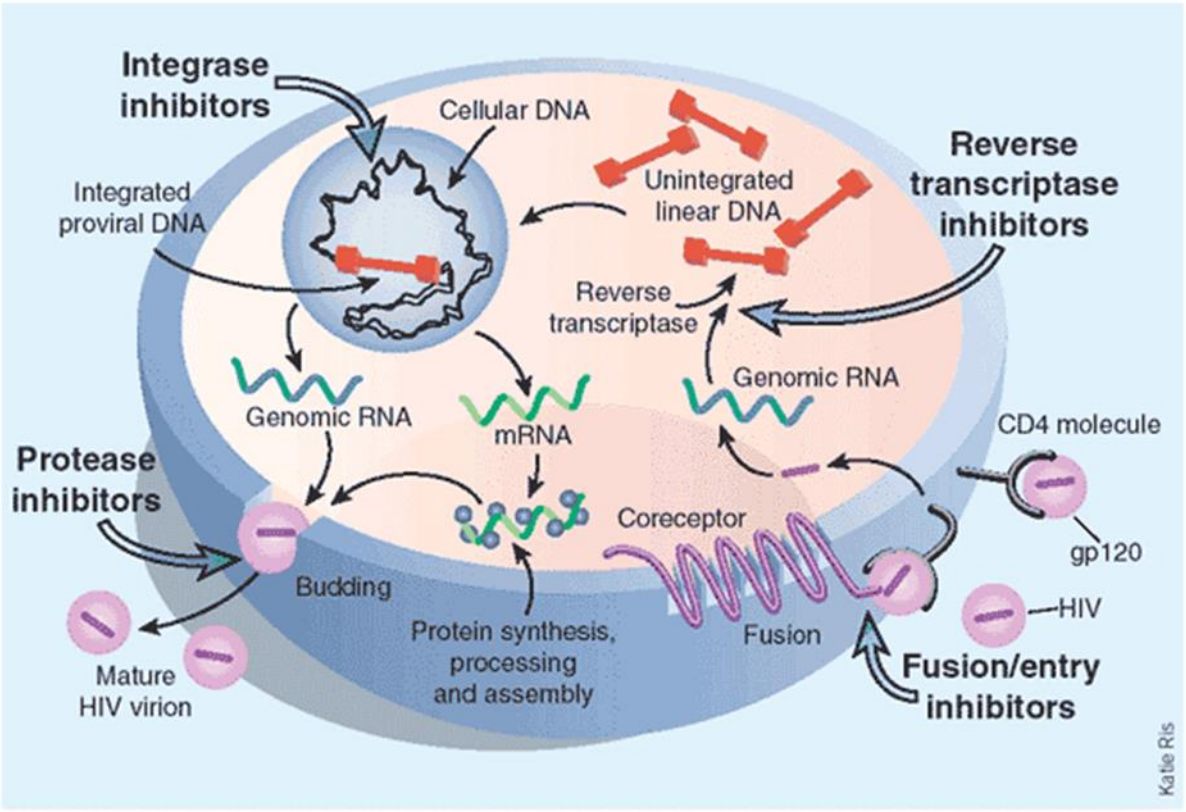

Figure 1.2. Summary of HAART target areas in HIV replication. Adapted from http://www.biology.arizona.edu/immunology/tutorials/AIDS/treatment.html

1.3.1. Effects of HAART

Despite lengthening the lifespan of HIV infected patients, HAART brought along with some serious health effects. These effects include lipodystrophy, dyslipidemia and insulin resistance. Lipodystrophy presents several features like peripheral fat loss and truncal fat accumulation (Aboud *et al.,* 2007). Of all HAART drugs, PIs emerged to be the ones playing a vital role in inducing those sides effects than the rest (Ismail *et al.,* 2009). A clinical study showed that HIV patients treated with PI have glucose intolerance and insulin resistance (Monier and Wicox, 2004).

1.4. Protease inhibitors

Protease in HIV is responsible for viral maturity by cleaving viral gag and gag-pol polyprotein precursors (Miller, 2001). Protease inhibitors are designed to compete with HIV aspartyl endopeptidase, the enzyme responsible for normal processing of gag and gag-pol HIV protein (Flexner, 1998). When bound to HIV protease active site, they attach to the HIV protease active

site, consisting of two flap domains, two core domains, and a terminal domain which altogether allows ligand binding in an induced-fit fashion (Rose *et al.,* 1998). This binding by PI to protease prevents the interaction of protease to its substrate which leads to failure in cleavage and results in immature virions (Temesgen *et al.,* 2006). It is known that PIs play a vital role in provoking side effects in the body as summarised below (Temesgen *et al.,* 2006).

Table 1.2 Common PIs and their major side effects.

Protease inhibitor	Major side-effects
Amprenavir	Severe rash, hyperglycemia, hypertriglyceridemia, and hypercholesterolemia
Atazanavir	Nausea, lipodystrophy, hyperbilirubinemia, diabetes, liver toxicity and kidney failure in some cases
Darunavir	Nausea, lipodystrophy, fever, stomach pain and abnormal liver function in some cases
Fosamprenavir	Raised lipids, dizziness, tiredness and lipodystrophy
Indinavir	Insulin resistance, nephrolithiasis, hyperglycemia
Kaletra	Diarrhoea, hyperglycaemia, hepatotoxicity
Nelfinavir	Diarrhoea hyperglycemia
Ritonavir	Taste perversion, hyperglycemia, hepatotoxicity, diabetes
Saquinavir	Hepatotoxicity, hyperglycaemia
Tipranavir	Hepatotoxicity, rash, hyperlipidaemia

1.5. Insulin resistance

Insulin resistance is a state of increased insulin concentration needed for a normal biological response; including glucose transport into muscle and fat cells, also suppression of glucose production via gluconeogenesis in the liver (Olefsky, 1997; Aboud *et al.,* 2007).

1.5.1. The insulin signal pathway

The insulin signal pathway is a type of negative feedback mechanism that is activated by a high glucose level in the bloodstream. In a case of high glucose level, from pancreas insulin is secreted into the bloodstream where it binds to its receptor, a heterotetrameric (2 α- and 2 β-subunits) and ligand-activated tyrosine kinase. Once attached to the receptor, the β-subunits of the receptor autophosphorylates on the tyrosine residue (Figure 1.3).

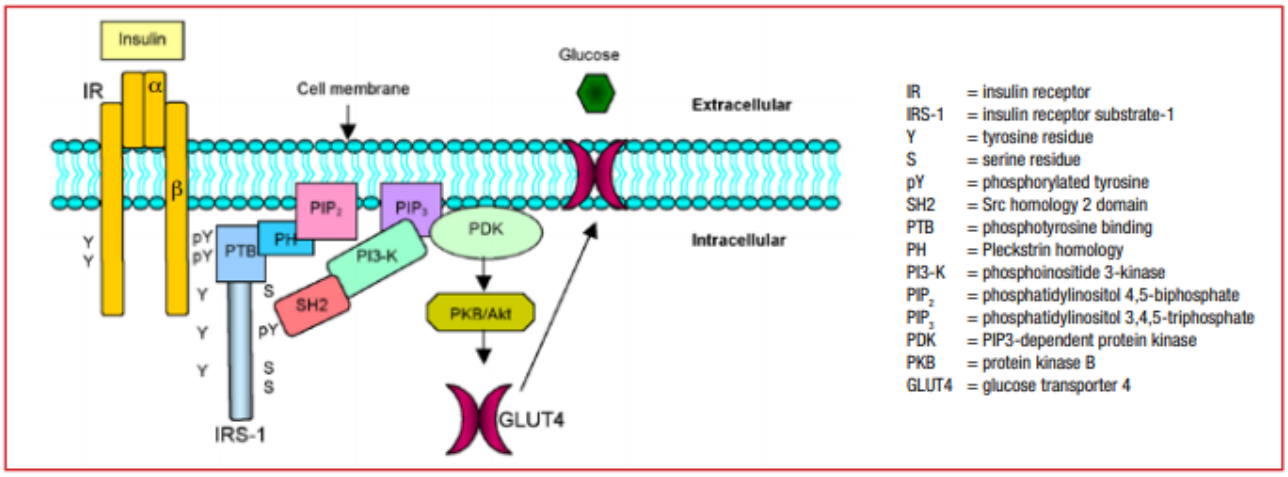

Figure 1.3. The insulin signal pathway*. Adapted from Ismail et al ., 2009.*

The process subsequently activates the intrinsic tyrosine kinase domain that then insulin receptor substrate -1 (IRS-1) phosphorylation. The phosphotyrosine residues typically interact with a protein domain, an Src homology 2 (SH2) domain with a high affinity and specificity. The phosphorylated IRS-1 in tyrosine residue attaches to the SH2 domain of the phosphoinositide 3-kinase (PI3-K) which leads to its activation and conversion of phosphatidylinositol 4,5-bisphosphate (PIP_2) to phosphatidylinositol 3,4,5-triphosphate (PIP_3). Bound PIP_3 causes the translocation of both PIP_3-dependent protein kinase (PDK) and Akt; this allows the phosphorylation and activation of Akt by PDK. This activation of Akt is crucial for the final step in glucose transport. The Akt activation results in the translocation of glucose transporter 4 (GLUT4) to the cell membrane from the cytoplasm to assist in the uptake of extracellular glucose (Fig 1.3).

1.5.2. Mechanism of insulin resistance

Multiple factors cause insulin resistance, and many studies have been done to understand the mechanism of how it is generated. Some mechanisms of insulin resistance have been discussed below:

1.5.2.1. SH_2B and APS

The Src homology 2B (SH2B) is a family of three members; SH2B-1 (PSM), SH2B-2 (APS) and SH2B-3 (Lnk), characterised by a pleckstrin homology (PH) domain and SH2 domain (Rui, 2014). The PSM homolog is located in the cytoplasm and contains a nuclear localisation sequence (NLS) vital for nuclear translocation (Maures *et al.,* 2009). A high titer is mostly observed in the

adipose tissue, skeletal muscle, liver, and pancreas, and regulated by hormones and nutrients signal (Ren *et al.,* 2007). Gutierrez-Aguilar and co-workers observed that there is a downregulation of PSM in rats fed with high-fat diet (Gutierrez-Aguilar *et al.,* 2012).

PSM bind to insulin receptors through the SH2 domain (Riedel *et al.,* 1997). An over-expression of PSM enhances the ability of insulin to phosphorylate tyrosine residue in IRS (Duan *et al.,* 2004). The PSM homolog protects IRS proteins against de-phosphorylation by directly binding to tyrosyl phosphorylated IRS and thus prolonging the ability of IRS to activate downstream pathways (Morris *et al.,* 2009). Knocking out PSM in mice led to the development of hyperglycemia, hyperinsulinemia and insulin resistance (Duan *et al.,* 2009).

Also, impaired insulin signaling in skeletal muscle, adipose tissue and liver in PSM knock out mice showed symptoms of hepatic steatosis and lipid accumulation in skeletal muscle (Duan *et al.,* 2009; Ren *et al.,* 2005). In a regular diet, PSM is not responsible for insulin sensitivity and metabolism of glucose, but it promotes insulin signaling and metabolism of glucose and lipid in obese subjects (Rui, 2014). Another SH2B homolog, APS, binds to insulin receptor via SH2 domain. Insulin activates the phosphorylation of APS in tyrosine residue in adipocytes. Overexpression of APS prolongs the insulin-stimulated phosphorylation of tyrosine residue in the insulin receptor and IRS protein (Ahmed and Pillay, 2003).

1.5.2.2. Phosphorylation of serine 307 on IRS-1

During insulin signaling, IRS-1 is directly phosphorylated in some specific residues, which serve as a hub for insulin signal, to perform metabolic control through protein kinase B (PKB). It plays a crucial role as a target for insulin signal modification through the cross-talk with other pathways. Phosphorylation of serine 307 inhibits the insulin signal pathway by either interference with insulin receptor phosphorylation, binding to downstream signaling intermediates and by increasing IRS-1 degradation (Aguirre *et al.,* 2000a; 2002b). In some isolated cases, serine 307 phosphorylation has been shown to increase the tyrosine phosphorylation in IRS-1 responding to insulin and therefore upregulate insulin signaling (Luo *et al.,* 2007). It has been demonstrated that this phosphorylation blocks phosphorylation of tyrosine residue from de-phosphorylation and subsequently inactivates IRS-1 (Paz *et al.,* 1999).

1.5.2.3. SOCS-1 and -3

The suppressor of cytokine signal (SOCS), also called Janus family kinase binding protein (JAB), is a family of eight proteins (SOCS1-7 and CIS) characterised by a central SH2 domain. The SH2 domain, that binds to phosphorylated tyrosine, a conserved C-terminal SOCS box, which regulates a proteasomal degradation, and NH2 terminal (Howard and Flier, 2006; Hilton *et al.,* 1998). Activated by cytokines, they interact with Janus activated kinase (Jak) or directly bind to cytokine receptors and proteasomal degradation of signaling protein through SOCS box complex, they act as negative feedback of cytokines and inhibit inflammation signal transduction (Howard and Flier, 2006). The SOCS-1 and SOCS-3 are the most studied and have a higher impact on insulin resistance.

Three mechanisms on how SOCS induces insulin resistance have been revealed: 1) by competing with insulin to bind to activated insulin receptors, 2) by degrading IRS proteins and 3) by inhibiting the activity of insulin receptor tyrosine kinase (Lebrun and Van Obberghen, 2008). Increased levels of inflammation, SOCS-3 is overexpressed in the hypothalamus, adipose tissue, and liver (Bjorbaek *et al.,* 1998; Emanueli *et al.,* 2001; Senn *et al.,* 2003). It was shown that in the absence of over inflammation, SOCS-3 expression in skeletal muscle is low (Alexander and Hilton, 2004). In a study by Emanuelli *et al.* (2000) in 3T3-L1 adipocytes, it was found that insulin induces SOCS-3 expression and its transportation to the plasma membrane.

Genetic deletion of SOCS-3 in a mouse liver showed an increase in insulin signaling due to elevated expression of IRS-1 phosphorylation, showing the negative role SOCS-3 plays in the insulin signaling (Torisu *et al.,* 2007). Its expression is upregulated in the skeletal muscle of obese insulin resistance mice, showing its role in obese-induced insulin resistance (Ueki *et al.,* 2004a). The SOCS-1 and -3 proteins over-expressed in the liver by adenoviral construct have been shown to decrease IRS expression and phosphorylation and attenuate PI3K activity (Ueki *et al.,* 2004a). It also induces the expression of SREBP-1C; thus, the expression of SOCS-1 and -3 in the liver induces glucose intolerance and systematic insulin resistance (Ueki *et al.,* 2004b).

Jorgensen *et al.* (2013) concluded that in obesity, SOCS-3 in the muscle contributes on insulin resistance and impairs glucose homeostasis which co-relates to the finding by Yang *et al.,* (2012) that skeletal muscle SOCS-3 is responsible for the muscle and systematic insulin resistance. This protein may also affect insulin signaling by antagonising AMPK signaling (Fisher

et al., 2002). Also, SOCS-3 regulates metabolism through leptin signaling inhibition (Dunn *et al.,* 2005).

1.5.2.4. TNF-α

Tumour necrosis factor-α (TNF-α) is a pro-inflammatory mediator which induces inflammation in vital organs (Akash *et al.,* 2013). It is important in insulin resistance manifestation by inducing oxidative stress and other metabolic pathways (Akash *et al.,* 2017). TNF-α also regulates apoptosis differentiation and cell recruitment (Ehlers, 2003). With the help of tumour necrosis factor receptor-1 (TNFR-1), TNF-α activates and recruit immune cells and propagate the inflammation. It also activates transcriptional pathways that induce oxidative stress which, together with inflammation interacts to promote cell degeneration (Fischer and Maier, 2015). In insulin resistance development, TNF-α prevents the expression of GLUT4 in adipose tissue and cardiac muscles (Huang and Czech, 2007). It also activates the IRS-1, which inhibits insulin receptor and downstream signaling of PI3K activity (Fasshauer and Paschke, 2003).

Dong and co-workers reported that administering TNF- α in cells, show an impaired insulin action compared to the non-administered counterpart (Dong *et al.,* 2015). Other mechanisms include downregulation if IRS-1, GLUT4, CEBP-PPAR, perilipin, and Acrp30 (Akash *et al.,* 2017). It also lowers oxidation of fatty acid, thus leading to elevated plasma FFA (Ruan and Lodish, 2003). Alteration of lipid metabolism induced by TNF- α in adipose tissues results in insulin resistance. TNF can also induce lipoproteins lipase- α to start lipolysis in adipose tissues. Lipolysis in the adipose tissue results in a high amount of non-esterified fatty acids leading to insulin resistance (Kern *et al.,* 2001).

In the state of obesity, TNF- α contributes to the development of insulin resistance, as high levels have been observed (da Rocha *et al.,* 2014; Carter-Kent *et al.,* 2008). This is achieved by induction of oxidative stress and oxidative stress-related such as inhibitor kappa beta kinase beta (IKK-β), JNK and *NFκB* pathway (Shoelson *et al.,* 2006). Activated JNK can moreover induce the production of TNF- α in the liver, adipocytes and muscle tissues (Ozcan *et al.,* 2004). Subjects undergoing PI and NRTIs treatment shows increased TNF-α expression (Vigouroux *et al.,* 2003).

1.5.2.5. The *NFκB* pathway

The *NFκB* pathway is a signaling pathway that is responsible for inflammation, apoptosis, carcinogenesis and oxidative stress. Its activity is found in vast cells, including adipocytes and macrophages (Hayden and Ghosh, 2008; Shoelson *et al.,* 2006). There are five members of the *NFκB*, namely RelA, RelB, c-Rel, *NFκB*1 (p105 generating p50 by co-translational modification) and *NFκB*2 (p100 generating p52 by co-translational modification), and they all share Rel homology domain (May and Ghosh, 1998; Huang *et al.,*2013). In a cell, these proteins are bound to their inhibitory molecules from the inhibitor of *NFκB* (IκB) family of protein characterised by ankyrin repeats (Hoesel and Schmid, 2013). The *NFκB*1 and *NFκB*2 do not have transactivation domain, unlike other *NFκB* forms, and when bound to gene promoter, they act as transcriptional repressors, (Hayden and Ghosh, 2012). Still, when bound to a member with the transactivation domain, it constitutes a transactivation activator (Hoesel and Schmid, 2013). Mice with *NFκB*1 knockout has shown the disappearance of transcription activity (Bohuslav *et al.,* 1998).

The general activation is by a release IκB from the molecule or by the cleavage of the inhibitory ankyrin repeats domain by the proteasomal degradation of the inhibitor or partial degradation of precursors (Hoesel and Schmid, 2013). The IκB kinase (IKK) (IKK-α and IKK-β) play a role in catalysis of a substrate recognition site. There are three activation pathways; the canonical pathway, mediated by toll-like receptors (TLR), interleukin-1 receptors (IL-R), TNF-receptor (TNFR) and antigen receptors. This stimulation leads to activation of the IKK complex, which in turn phosphorylates IκKα by IKK2 (Perkins and Gilmore, 2006).

Different types of receptors mediate the non-canonical pathway. These include B-cell activation factor receptors (BAFFR), lymphotoxin β-receptors (LTβR) and CD40. The activation of these receptors, in turn, leads to the activation of *NFκB* inducing kinase (NIK), which phosphorylates and activates IKK1. The activation of IKK1 induces the p100 phosphorylation resulting in partial degradation to p52 (Xiao *et al.,* 2001). The atypical activation pathway, mediated ataxia telangiectasia mutated (ATM)-dependant phosphorylation of *NFκB* essential modulator (NEMO) after genotoxic stress (DNA double-stranded break) (Huang *et al.,* 2003).

Bohuslav and co-workers elucidated that there is an increase of *NFκB* expression in *NFκB*1 inhibitor knockout mice (Bohslav *et al.,* 1998). In a cellular model, Ruan and co-workers (2002,2003), concluded that *NFκB* inhibits the adipocytes differentiation and functioning in the

signal pathway of TNFα (Ruan *et al.,* 2002, 2003). The proposed molecular mechanism is related to PPARγ activity by *NFκB*. Other models of inhibition include PPARγ suppression in mRNA level, DNA binding activity, and interaction with transcriptional co-activators (Ruan *et al.,* 2002; Suzawa *et al.,* 2003; Gao *et al.,* 2006).

Previous studies have suggested that *NFκB* may inhibit insulin sensitivity by inducing inflammatory cytokines or by inhibiting PPARγ (Shoelson *et al.,* 2006; Tan *et al.,* 2012). Other studies by Schitz and Baeuerle in 1991, suggested that inflammation is increased as a result of increased *NFκB* activity by a p50 gene knockout suggesting that p50 expression hinders *NFκB* activity (Schitz and Baeuerle, 1991). Adipose tissue inhibition contributes to high energy expenditure through the suppression of PPARγ inhibition in transcriptional level (Tang *et al.,* 2010). This suppression may be the mechanism for adipose tissue deficiency in p50 knocked out mice (Tang *et al.,* 2010).

Studies by Tang and co-workers suggested that there are two different activity of inflammation that regulates metabolism. It can be either by inhibition of insulin sensitivity, which makes a negative feedback mechanism or by inducing energy expenditure (Tang *et al.,* 2010). It was concluded that inflammation induced by *NFκB* has a crucial activity in inducing energy expenditure in p50 knockout mice (Tang *et al.,* 2010). In murine studies, *NFκB* appeared to inhibit PPAR-γ-mediated effects, which later inhibits adipogenesis and promote osteogenesis (Suzawa *et al.,* 2003).

According to two independent studies (Arkan *et al*., 2005; Cai *et al*., 2005), using selective transgenic expression and IKKB knockout in the liver respectively, proved that NFκB is a significant factor in insulin resistance. Overexpression of IKKB in the liver mimics a high-fat diet-induced insulin resistance while the expression of IkBa in liver reverses type 2 diabetes. There are a number of studies that show the activation of NFκB by hyperglycemia which includes but not limited to (Suzawa *et al*., 2003), shows that from a mesenchymal cell derived from bone marrow, the activation of NFκB antagonises the function of PPARγ, a receptor that regulates lipid and glucose homeostasis. In another study by Hotamisligil in 1995, it was shown that TNFα is overexpressed in obese animals while insulin sensitivity can be achieved by its neutralisation (Hotamisligil *et al*., 1995). The NFκB is not only implicated in type II diabetes but also in its complications, including, diabetic cardiomyopathy, diabetic retinopathy, diabetic nephropathy, and diabetic neuropathy.

A. Diabetic cardiomyopathy

Diabetic cardiomyopathy is the leading cause of death in diabetic patients and can be caused by many factors, including insulin resistance. Diabetes induces oxidative stress, which leads in the increased levels of advanced glycation end products (AGE), then overexpression of receptor for AGE (RAGE) and galectin-3 levels. All these lead to increased TNFα and its receptor TNFα-R1, suggesting that these events impair cardiac-specific transcription factors. Also, these lead to the reduced expression of myosin heavy chain genes in the left ventricle (Patel and Santani, 2009).

Studies also show that the activation of NFκB downstream genes triggers other pathways through the production of proinflammatory cytokines like TNFα, which is involved in heart damage. TNFα again triggers NFκB to amplify the detrimental effects in the heart (Esposito *et al.,* 2003). This activation still leads to a switch in cardiac myosin heavy chain gene expression (Aragno *et al*., 2006).

B. Diabetic retinopathy

It is regarded as one of the leading causes of blindness and vision impairment globally (Patel and Santani, 2009). In diabetic patients, accumulation of AGE and RAGE increases retinal microvasculature. AGE can also be irreversibly formed and build-up in retinal capillary cells, increasing ROS formation, thus activating NFKB and forcing more cellular damage (Mohamed *et al*., 1999). Activation of NFκB also results in overexpression of free radicals and interleukins, which creates a continuous feedback loop by releasing more ROS (Vissilakopoulos *et al*., 2003). Other studies show an increase in intraocular levels of monocytes chemotactic protein-1 (MCP-1) which increases proliferative diabetic retinopathy (PDR) (Harada *et al*., 2003). Studies by Harada in 2003, suggests that MCP-1 regulated by NFκB is involved in the pathogenesis of PDR.

C. Diabetic nephropathy

Diabetic nephropathy is associated with renal failure and poses a threat in death related to heart failure in diabetic patients (Patel and Santani, 2009). It has been reported before that the nuclear translocation of NFκB from the nucleus is demonstrated in diabetic nephropathy (Cohen *et al*., 2002; Sakai *et al*., 2005). In diabetic patients, due to high levels of ROS and

cytokines, leukocytes are highly activated, which later releases superoxide radicals and proteases that are known to promote oxidative stress (Patel and Santani, 2009). Also, elevated glucose concentration generates ROS in mesangial cells.

There are a number of NFκB-dependent pathways that play a role in macrophage infiltration and kidney injury. It was shown that there was a high expression of p65, an NFκB subunit, in diabetic animals due to increased MCP-1 gene expression and macrophage infiltration (Cha *et al.*, 2005). NFκB is regulated by angiotensin II (Ang II), a cell proliferation, apoptosis, fibrosis and inflammation through NFκB (Esteban *et al*., 2003). Ruiz-Ortega *et al.* (2001) concluded that AngII activates renal NFκB via both AT_1 and AT_2 receptors (Ruiz-Ortega *et al.,* 2001).

D. Diabetic neuropathy

Neuropathy refers to the loss of pain perception, which triggers a series of events that leads to chronic diabetic ulcers (Patel and Santani 2009). Also, hyperglycemia activates diabetic neuropathy by hyperexpression of proinflammatory cytokines like IL-6 and TNFα (Mattson and Camandola, 2001, Vincent *et al.,* 2002). In clinical trials, it has been shown that α-lipoic acid, an NFκB suppressor, diminishes symptoms in somatic and autonomous neuropathy and reduces blood flow (Haak *et al.*, 1999; Ziegler *et al*., 1999).

1.5.2.6. JNK-1

c-Jun kinase 1 (JNK-1) is a member of the mitogen-activated protein kinases (MAPK) family that holds a unique feature than the rest since it can induce a response to cellular stress than to mitogen (Chang and Karin, 2001). Three JNK isoforms have been identified, and those are JNK-1, JNK-2, and JNK-3. The JNK-1 and-2 are ubiquitously expressed in the body, while JNK-3's expression is confided in some parts of the body, i.e. brain, testis and pancreatic β-cells (Solinas and Karin, 2010). These proteins play a critical role in cell response to stress, and their activities have been involved in the pathogenesis of obesity-induced insulin resistance (Solinas and Becattini, 2017).

In separate studies, Hotamisligil and co-workers in 1993; and Tanti and co-workers in 1994, led to the understanding of the mechanism by which JNK induces insulin resistance. Tanti reported that serine/threonine phosphorylation of IRS-1 leads to defective IRS1 and reduces

phosphatidylinositide 3 kinase (PI3K) AKT signaling in response to insulin receptor activation (Tanti *et al.,* 1994). Hotamisligil a year before had reported that, TNF-α expression is elevated in adipose tissue of obese insulin-resistance rodents in contrast to those slim controls and that neutralisation of TNF-α improves insulin sensitivity in obese insulin resistance rats (Hotamisligil *et al.,* 1993).

The above two studies showed that serine/threonine kinases induced by TNF-α and inflammation, including JNK promote insulin resistance by direct phosphorylation of IRS molecules (Solinas and Karin, 2010). Treatment of cells with anisomycin, a potential JNK inducer, showed a reduction in of IRS-1 and IRS-2 tyrosine phosphorylation in response to insulin which was followed by the increase in serine/threonine phosphorylation in IRS-1 and -2 (Aguirre *et al.,*2000). It was shown that the JNK phosphorylates serine-307 in IRS-1 and that this phosphorylation inhibits the interaction of IRS-1 and insulin receptor in response to insulin (Aguirre *et al.,* 2000a; Aguirre *et al.,* 2002b). It was also shown that JNK activity in mouse muscle, fat and liver is increased in obese mice (Hirosumi *et al.,* 2002).

The study by Sabio and colleagues was conducted to examine the role of JNK-1 in adipocytes using a mice model lacking *Jnk1* gene, a gene responsible for JNK-1 expression (Sabio *et al.,* 2008). The mice were protected against insulin resistance development by feeding them a high-fat diet (Sabio *et al.,* 2008). Furthermore, it was also elucidated that this effect is tissue-specific due as *Jnk1*-deficiency in adipocytes did not cause any change in insulin sensitivity in the muscle, but improved liver insulin sensitivity (Sabio *et al.,* 2008). C-Jun kinase 1 is also shown as a requirement for adipocytes interleukin 6 (IL6) in response to a high-fat diet, as there was a drastic decrease in the expression of IL6 in mice fed with a high-fat diet (Sabio *et al.,* 2008) Mouse lacking *JNK-2* and only one allele also showed protection from diet-induced obesity and insulin resistance elucidating that JNK-2 is also involved in the obesity-induced insulin resistance (Tuncman *et al.,* 2006)

1.5.2.7. GLUT4

Glucose transporter isoform 4 (GLUT4) is insulin-responsive facilitative glucose transportation highly expressed in skeletal, adipose and cardiac muscle cells (Atkinson *et al.,* 2013). The GLUT 4 is located in the organelles such as Golgi apparatus and endosomes in a basal state, GLUT4 translocates to the plasma membrane in response to insulin. That is where GLUT 4 takes up extracellular glucose for storage and recycling (Leto and Saltiel, 2012). The transporter GLUT4

is known for its role in glucose homeostasis, and this has been shown by enhanced insulin sensitivity in response to increased GLUT4 expression (Ikemoto *et al.*, 1995).

In obesity, GLUT4 expression is compromised, leading to insulin-resistant glucose transport (Garvey *et al.,* 1991). It has been observed that in insulin resistance state, there is an impaired skeletal muscle glucose transport suggesting its role in insulin sensitivity (Pendergrass *et al.,* 2007). In a study by Tsao *et al.* (1996), it was elucidated that GLUT4 improves insulin sensitivity in mice. In one study, it was shown that loss of GLUT4 in cell surface in response to insulin is correlated with insulin resistance (Atkinson *et al.*, 2013).

Protease inhibitors play a role in the loss of glucose uptake by GLUT4 into the cell, as observed in one study (Murata *et al.,* 2000). In the study, 3T3-L1 adipocytes treated with indinavir shows a 63 % inhibition of GLUT4 after only 6 minutes of treatment (Murata *et al.,* 2000). This inhibition is more likely to be the direct cause of insulin resistance in HIV-infected persons and diabetes results when pancreatic cells are unable to compensate for insulin (Murata *et al.,* 2000).

A GLUT4 knocked out mice showed insulin resistance and devoid fat tissue in one study (Katz *et al.*, 1995). This observation suggests that GLUT4 activity on its own is required in adipogenesis. Furthermore, PI accounts for lipodystrophy (Murata *et al.,* 2000). It has been suggested that PI interferes with adipogenesis in cell culture which is in line with findings by Carr and colleagues in the previous year (Zhang *et al.,*1999, Carr *et al.,* 1998).

1.6. The role played by protease inhibitors in insulin resistance

Protease inhibitors are said to play a crucial role in insulin resistance. Ismail *et al.* (2009) outline a possible mechanism whereby PI leads to insulin resistance viz. (1) impairment of distal steps in the insulin signaling pathway, (2) impairment of proximal steps in the insulin signaling pathway and (3) induction of other factors involved in insulin resistance by PI.

1.6.1. Impairment of distal steps in the insulin signaling pathway

Studies by Murata *et al.* (2000) demonstrated that PIs suppress glucose uptake without disturbing GLUT4, a major transporter of glucose into adipose tissue and skeletal muscle (Mueckler, 2001). In subsequent studies by Rudich *et al.* (2001), treatment of 3T3-L1 adipose

tissues treated with 10 µM of nelfinavir impaired GLUT4 translocation and glucose. This was due to the ability of nelfinavir to inhibit the stimulation of PKB/Akt serine-437 phosphorylation. This inhibits insulin signal pathway by binding to downstream signal intermediates. It was also noticed that nelfinavir decreases the expression of perilipin, a lipolysis regulator (Rudich *et al.,* 2001). In independent studies by Ben-Romano *et al.* (2004) and Rudich *et al.* (2003), it was revealed that nelfinavir induces insulin resistance by inhibiting both the recruitment and activation of PI3K, which leads to disrupted GLUT4 translocation, therefore, preventing glucose uptake.

Kachco *et al.* (2009) observed that PKB/Akt was inhibited after the generation of PIP_3, thus leading to a disturbed GLUT4 translocation. In the presence of nelfinavir, PKB was expressed and phosphorylated by PDK and induced GLUT4 translocation. This process meant that nelfinavir interfered with the sensing of PIP_3 (Kachco *et al.,* 2009). Nelfinavir also had more effects than their counterpart indinavir which only inhibits glucose uptake and not translocation (Ismail *et al.,* 2009). Nelfinavir also induces oxidative stress in adipocytes, which is responsible for causing insulin resistance (Ben-Romano *et al.,* 2006). This is due to the increase in reactive oxygen species concentration which oxidise and damage macromolecules (Nishikawa *et al., 2000).* Reactive oxygen species also act as a signaling molecules and activates stress sensitive pahway causing call damage (Evans *et al.,* 2003).

1.6.2. Impairment of proximal steps in the insulin signaling pathway

Some evidence pointed to PI having more proximal effects on the insulin signaling pathway. Studies showed that indinavir decreases about 30-60 % tyrosine phosphorylation of IRS-1 in HepG2 hepatoma cells and it was linked to decreasing in PI3K activity with no effect on insulin binding affinity which suggest that indinavir influences IRS-1 phosphorylation associated with PI-3 pathway (Schutt *et al.,* 2000; Virkamaki *et al.,* 1999). Ritonavir showed a decreasing number of insulin receptors, but not the binding affinity simultaneous with a decrease in IRS-1 phosphorylation in the tyrosine residues responding to insulin (Schutt *et al.*, 2000).

Another PI, lopinavir, inhibited IRS-1 phosphorylation in a study conducted in human adipocytes. This inhibition resulted in a decrease in glucose uptake in a concentration-dependent fashion (Djedaini *et al.,* 2009). It had been hypothesised before that lopinavir

decreased phosphorylation of IRS-1 directly and not affecting β-subunits in the insulin receptor. This means that PI affects early steps in the insulin signal pathway (Ismail *et al.,* 2009).

1.6.3. Induction of other factors involved in insulin resistance by PI

It has been observed that PI alter chemokines, cytokines or adiponectin production in human adipocytes and macrophages (Lagathu *et al.,* 2007). It has been shown that indinavir increased the expression of SOCS-1 in the liver, skeletal muscle and adipose tissues in a study conducted in rats (Carper *et al.,* 2008). The overexpression of SOCS-1 and TNF-α was associated with reduced expression of SREBP-1 and IRS-2, responsible for insulin action in the insulin pathway. TNF-α suppresses the functionality of IRS proteins to manifest insulin resistance (Ismail *et al.,* 2009). As observed by Carper and co-workers, TNF-α induces SOCS-1 expression. Of note, TNF-α activates other kinases including JNK and IKK, which leads to phosphorylation of IRS-1. These PI change adipose, adiponectin, and leptin gene expressions which results in repeated starving cycles and impaired fats storage (Chaparro *et al.* .2006).

1.7. Genome editing

Genome editing is a unique tool that researchers use to manipulate a gene or genome to create a new cell line, stain or organism. Three most common techniques of gene editing are employed in a wide range of science applications. These techniques are namely; transcription activator-like effector (TALE), a zinc-finger nuclease (ZFN) and Clustered regularly interspaced short palindromic repeats CRISPR associated protein 9, (CRISPR/Cas9).

1.7.1. TALENs

Transcription activator-like effector (TALE) are natural proteins obtained in plant pathogenic bacteria of genus *Xanthomonas.* During infection, the proteins are delivered to the plant cell through the type III secretion pathway (Bogdanove *et al*., 2010). Once in the cell, TALE enters the nucleus, bind effector-specific DNA sequence and transcriptionally activate gene expression, which increases plant susceptibility to pathogen colonisation (Christian *et al.*, 2010). They consist of 33-35 amino acid series repeats recognising a single base pair. TALE's

specificity largely depends on the repeat-variable di-residues (RVD), the two-hypervariable amino acid. TALE repeats are linked together to recognise contiguous DNA sequences.

TALE repeats have been made to fuse with effector domains to target genetic modifications, including nucleases (TALEN), transcriptional activators and site-specific recombinases (Miller *et al.,* 2011; Mercer *et al.,* 2012). Though it has shown advantages as compared to other technique before it, it has technical challenges due to identical repeat sequences. TALENs has been used in researches to compare gene function across related species such as *C. elegans* and *Caenorhabditis brisae* (Wood *et al.,* 2011). TALENs have shown the capability of correcting the underlying cause of disease, thus eliminating symptoms of genome modification (Gaj *et al.,* 2016).

1.7.2. ZFN

Zinc finger nuclease (ZFNs) are chimeric-engineered nucleases designed to target specific sequences in a genome. ZFNs have two modular domains, namely, DNA binding domain and DNA cleavage domain linked together via linker peptide that together mediates mutation (Durai *et al.,* 2015).

The functionality of ZFN is mainly derived from their conserved interaction between the domains and cognate DNA sequence. Each ZFN domain consists of two conserved Cysteines and two conserved Histidines, forming a Cyt_2His_2 chain in a short stretch of 30 amino acid (Klug, 2010). Those two conserved residues recruit zinc ion to fold peptides into tertiary conformation with anti-parallel beta-sheets containing Cysteine residues and Alpha helix containing Histidine residues (Rhodes and Klug, 1993). Each finger unit recognises 3-4 base pairs of DNAs and makes a base-specific contact through the interaction of its alpha-helix with a major groove of DNA. In the ZFN, DNA cleavage is mediated by the Folk domain, which belongs to the type of restriction endonucleases (Jabalameli *et al.,* 2015). For correct geometry, two ZFN must duly bind to the target sequence to allow proper dimer formation.

Zinc finger nuclease has been applied in research and medicine. To date, ZNF-induced HDR has been used to correct the disease-causing mutation associated with the X-linked severe combined immune deficiency (SCID) (Urnov *et al.*, 2005). It has also been used to introduce targ*et al*teration in plants including Arabidopsis and other crop species to allow the addition of

desired characteristics or phenotypes such as disease and herbicide resistance and high-quality food (Shukla *et al.,* 2009)

1.7.3. CRISPR/Cas9

Clustered regularly interspaced short palindromic repeats (CRISPR) CRISPR-associated nuclease 9 (Cas) is an adaptive immune system in bacteria and archaea which resists the virus via incorporating short repeats of the viral DNA into the bacterial genome (Horvath *et al.,* 2010). When a bacterial colony is transfected for a second time, transcripts of those repeats directs a nuclease to the complementary DNA (cDNA) from the invading virus and thus destroys the viral DNA.

The system has been observed in about 40 % and 90 % genomes sequenced in bacteria and archaea, respectively (Grissa *et al.,* 2007). CRISPR/Cas is classified into two super-classes; the class I which consist of standard and diversified type I, type III and a rare type IV and the class II which consist of type II, type V and type VI (Kira *et al.,* 2018). The distinct characteristic between the two classes lies on whether it uses a multi-subunit protein complex (class I) or single protein (class II) (Gleditzsch *et al*., 2019). The main six types of CRISPR-Cas system are determined by the signature Cas protein responsible for the target cleavage (Gleditzsch *et al*., 2019). The two classes and their types, subtypes and examples are summarised on Figures 1.4 and 1.5 respectively below.

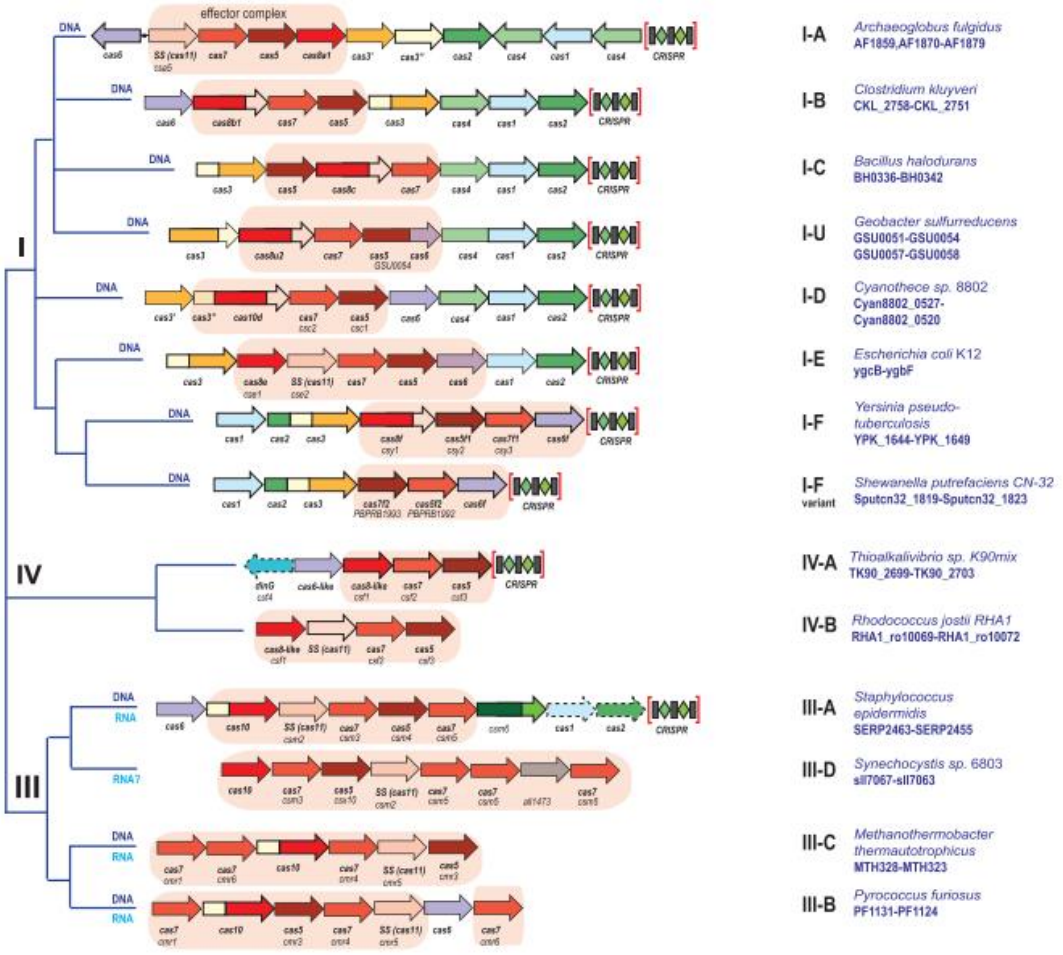

Figure 1.4. The class I CRISPR-Cas system*. A typical operon organisation is shown for each sub-type. Each subtype, a representative genome and respective gene locus is shown. Homologous genes are color-coded and identified by separate family names. Adapted from Makarova et al., 2018.*

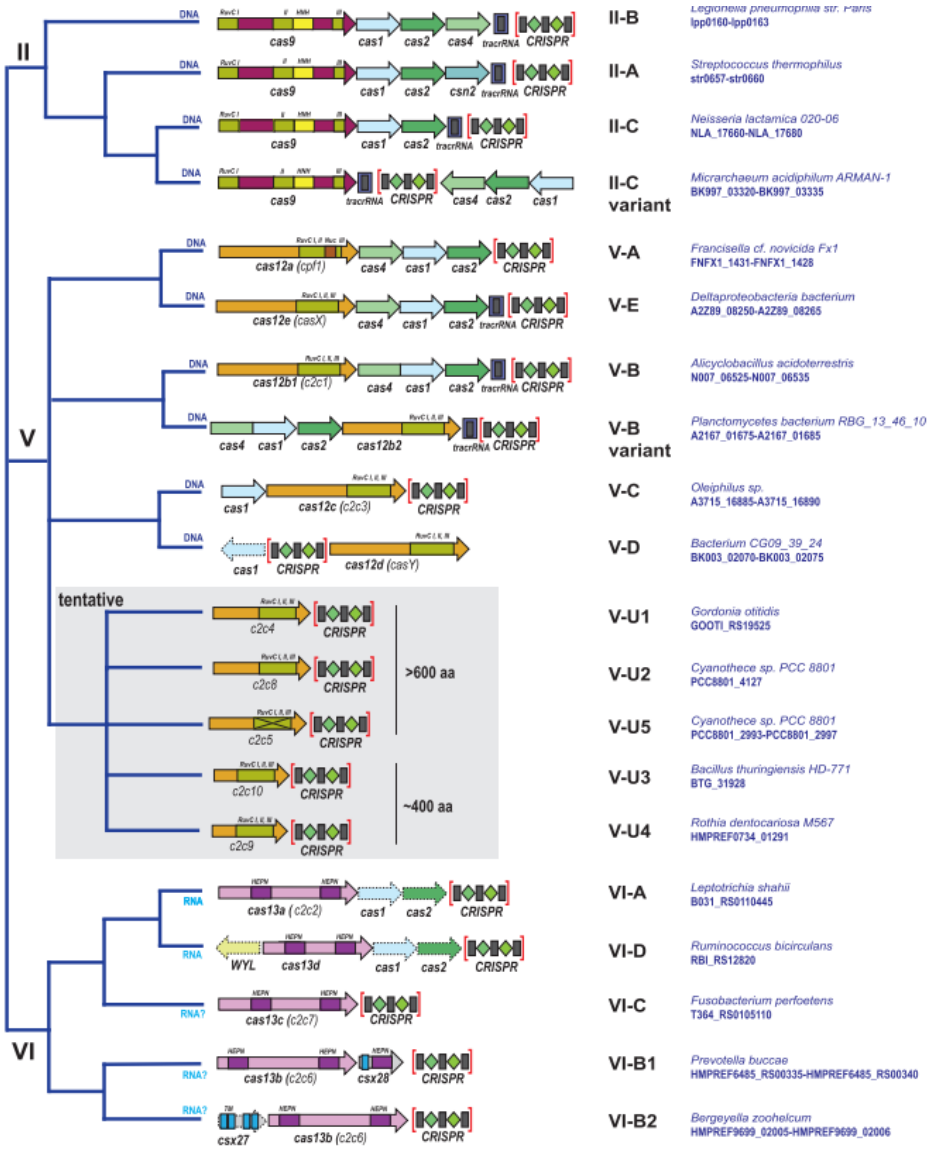

Figure 1.5. The class II CRISPR-Cas system*. RuvC I, RuvC II and RuvC III are three distinct motifs contributing to nuclease catalytic centre to cleave target DNA. Adapted from Makarova et al., 2018.*

This system works in three stages, acquisition, expression and target interference, as shown in Figure 1.5. In the acquisition, invading phage DNA, also called protospacer, is processed by Cas nuclease into small fragments of DNA, which then are incorporated into the CRISPR locus of the host genome as spacers. In response to the invasion, CRISPR-RNAs (crRNA) are expressed using the spacers processed in the acquisition stage as transcriptional templates. These crRNA guides Cas to cleave a target DNA sequence of invading phage (Zhang *et al.,* 2014). In the final stage, through the guidance of crRNA Cas proteins recognises the appropriate target and mediate the cleavage of the invading phage and by so doing protecting host cells from phage infection (Hsu *et al.,* 2014, Arneu *et al.,* 2010, Deltcheva *et al.,* 2011).

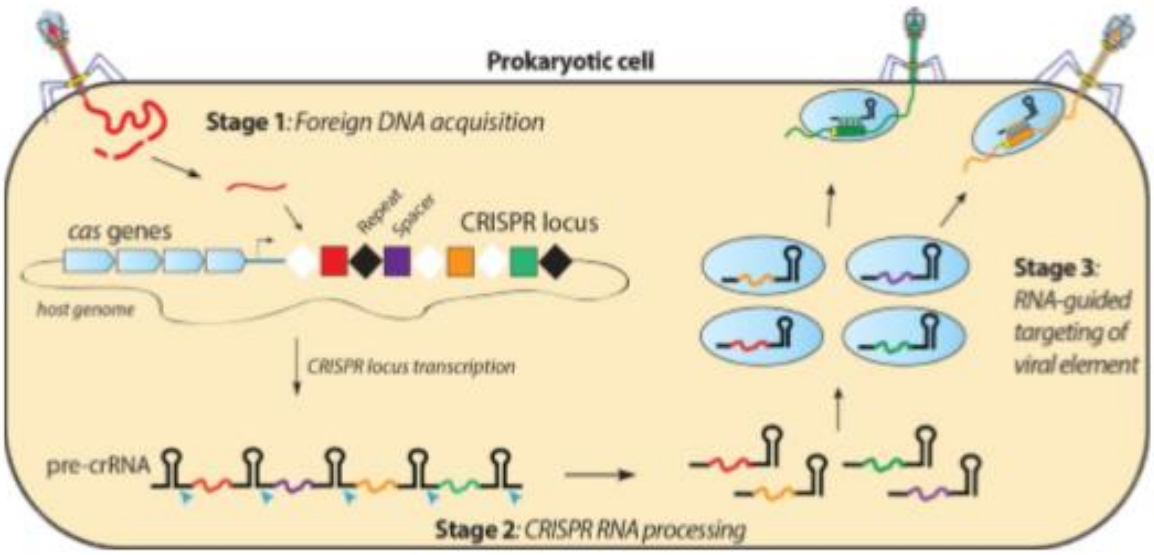

Figure 1.6: A typical sketch showing the innate immunity in the prokaryotic cell using CRISPR *(Doudna lab 2018, http://doudnalab.org/research_areas/crispr-systems/). When a bacterium gets attacked by a bacterial phage, the CRISPR system responses. CRISPR is composed of short palindromic repeats of DNA that have so-called spacers between each repeat. These spacers are unique. The Cas genes are different genes that associate with CRISPR and make Cas proteins. These spacers will function as the genetic memory for previous attacks in the bacteria and will either recognise the bacterial phage or be activated. If the spacer is activated, it will copy the foreign DNA into the CRISPR. This will give a library of short CRISPR-derived RNA (crRNAs) that will contain the complementary sequence to that of the invading nucleic acid (Jiang and Doudna, 2017).*

The CRISPR/Cas9 system has been adopted for genome engineering in the eukaryotic cell which can be achieved by three minimal components: Cas9, specificity-determining CRISPR RNA (crRNA), and an auxiliary trans-activating RNA (tracrRNA) (Mali *et al.,* 2013). In most cases, the tracrRNA and the crRNA are fused and generate single-guide RNA (sgRNA).

A typical sgRNA is a 20-nucleotide long sequence of DNA complementary to the targeted DNA followed by the protospacer adjacent motif (Anders *et al.,* 2014). It comprises of the seed sequence and non-seed sequence. The first 10-12 base pairs adjacent to PAM on the 3' end, the seed sequence' determines Cas9 specificity (Cong *et al.,* 2013). The seed sequence influences the specificity of Cas9-sgRNA binding.

The success of the system depends on the recognition of protospacer adjacent motif (PAM) element of foreign genetic materials, and the mechanism of recognition differs from species to other depending on which type the Cas protein falls under (Gleditzsch *et al.*, 2019). Protospacer adjacent motif is a short conserved sequence ranging from 2 – 5 bp located next

to target DNA which serves a purpose of discriminating between the 'self' and 'non-self' DNA increasing binding specificity (Westra *et al*., 2013).

For understanding the mechanism of PAM recognition, the Cas protein has been widely studied. For example, *Streptococcus pyogenes* Cas9 (SpCas9), which recognise 5'-NGG-3' PAM sequence has been studied in detail (Mojica *et al*., 2009; Karvelis *et al*., 2015; 2017). In those studies, crystal structure shows two major lobes; the recognition lobe (REC) and the nuclease lobe (NUC) that accommodate the sgRNA: DNA heterocomplex (Nishimasu *et al*., 2014). The binding of gRNA results in a conformational change on the SpCas9, which includes the formation of PAM interaction site (Anders *et al*., 2014). This rearranged protein is then competent for target recognition and interrogates DNA in the presence of correct PAM Sequence (Gleditzsch *et al*., 2019).

Two signature nuclease domains also characterise the Cas9; the RuvC and the HNH, which cleavage DNA strands that are complementary and non-complementary, respectively (Gasiunas *et al*., 2012; Jinek *et al*., 2012). Besides, SpCas9 also have a PAM-interaction domain have been shown to form a significant groove interaction with the non-target GG dinucleotides. The PAM recognition initiates stable R-loop formation and allosterically regulates dsDNA blunt cleavage in a fixed distance of 3 bp upstream of PAM (Palermo *et al*., 2017; Anders *et al*., 2014). This then means that PAM recognition is a prerequisite for SpCas9 activity (Sternberg *et al*., 2014; 2015)

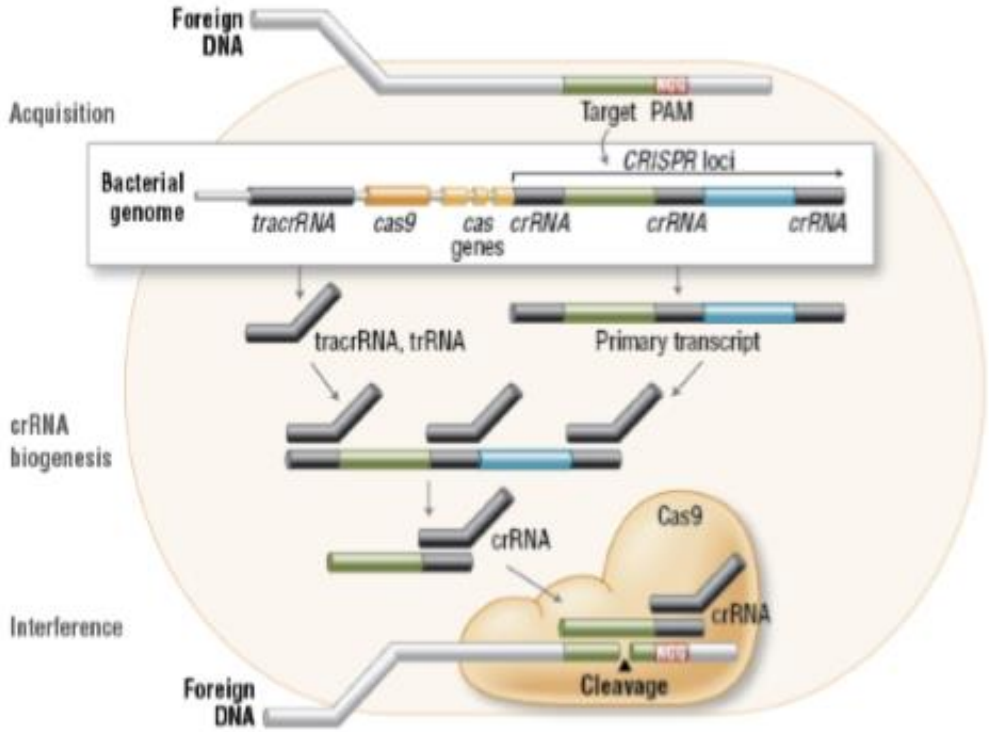

Figure 1.7.: Sketch showing the mechanism of CRISPR at a molecular level. If a bacterium gets attacked by a virus, two different types of short RNA will be produced when CRISPR loci are transcribed and processed into CRISPR RNA (crRNA) during crRNA biogenesis. crRNA will contain a sequence that will match the invading nucleic acid. These two RNAs will form a complex with a protein called Cas9 during interference phase. When the matching sequence is known as a guide RNA (gRNA) find its target within the viral genome, the Cas9 will cut the target DNA. This will disable the virus (Reis et al. 2014)

In most cases, gene knockout by CRISPR/Cas9 is achieved by inducing double-strand break (DSB). The subsequent DNA repair process by the cell using either nonhomologous end-joining (NHEJ)- mediated or by homology-directed repair (HDR) although it is not limited to (Hsu *et al.,* 2014; Hess *et al*., 2017). The NHEJ repair induces the accumulation of small insertions or deletions (indels) because it rapidly ligates DBS. Thus it is error-prone (van Overbeek *et al.,* 2016, Zhang *et al.,* 2014). If ever those indels lie on the exon, the open reading frame (ORF) will be disrupted. On the corresponding gene, thereof will be a nonsense-mediated decay which leads to renege of translation or transcription (Hsu *et al.,* 2014). These mutations can be used to disrupt the function of the target gene or even genetic element.

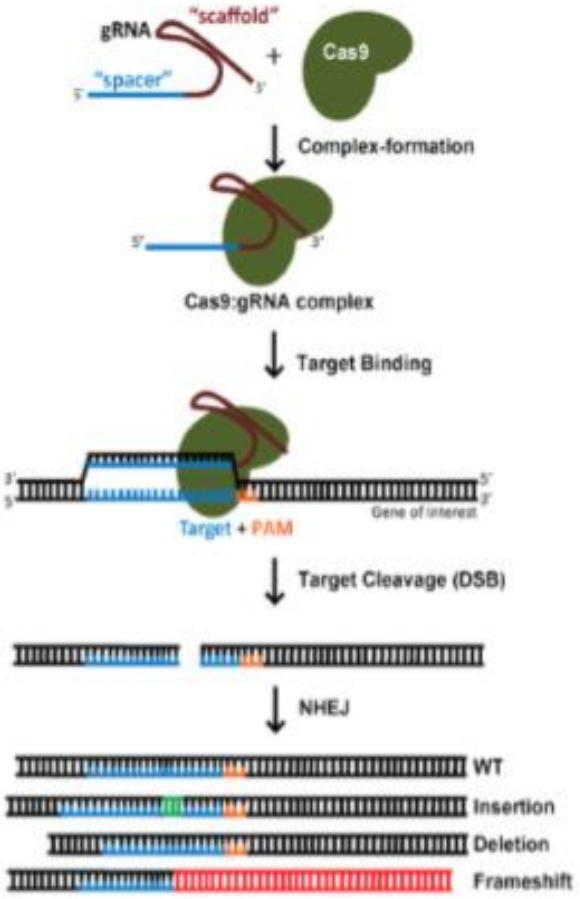

Figure 1.8: A sketch showing NHEJ pathway and the probable results. *Guide RNA (gRNA) and Cas9 will form a complex which will lock on to a short protospacer adjacent motif (PAM). Cas9 has two active sites, whereas each of these sites will cut one of the complementary DNA strands. The double-strand break will usually be repaired by the non-homologous end joining (NHEJ) pathway. This pathway will often lead to different mutations as small deletion, insertion or frameshift (Addgene 2017)*

The HDR mediated repair, on the other hand, it is more complicated as compared to NHEJ as it requires a homology-containing donor DNA sequence as a repair template. Grarts and co-workers managed to edit a genome through co-injecting Cas9 and two gRNA targeting the 5' and 3' sequence; and single-strand oligodeoxynucleotide template (Grarts *et al.*, 2013). The HDR mediated repair is mediated in the S- and G2 phase in the cell (Salsman and Dellaire, 2016).

The biggest challenge of the system is off-targets. These off-target effects occur since the 20-bp targeting sequence in the guide RNA (gRNA) may be elsewhere in the genome (Ran *et al.,* 2013). Some methods developed to detect off-targets. T7 endonuclease I assay have been

used, previously, however, it offers reduced sensitivity and not cost-effective for extensive scale screening (Cho *et al.,* 2013). Advanced methods have been developed, which includes deep sequencing, *in silico* prediction tools and CHIP-seq (Ran *et al.,* 2013).

Strategies to minimise off-target effects have been reported (Kim *et al.,* 2015). Firstly, gRNA can be altered by truncating the gRNA at the 3' end, shortening the region complementary to the target site at the 5' end or by adding two guanine nucleotides at the 5, end of the gRNA. This alternation has been reported that it improves target specificity and decreases undesirable mutagenesis at the off-target site by 5000-fold. Secondly, Cas9-sgRNA concentration can be controlled by titrating the amount of Cas9, and sgRNA delivered (Kuscu *et al.,* 2014). Thirdly, in place of the wild-type Cas9, a D10 mutant nickase version can be used instead (Ran *et al.,* 2013).

The latter uses a non-DSB-mediated genome editing but a base editing system that does not involve DSB. These are divided into two, namely the cytosine base-editor (CBE) and adenosine base-editor (ABE) (Chen *et al*.,2019). Although they are useful, they cannot wholly replace DSB-based editing as they cannot achieve gene insertion and gene replacement (Chen *et al*., 2019)

Also, in a study by Zhang and colleagues generated a DNA-free edited wheat by bombarding in vitro transcripts of Cas9 and sgRNA into an immature embryo (Zhang *et al*., 2016). Although there was a reduction in edition efficiency might be due to RNA instability, there was a reduction in off-target effects (Zhang *et al*., 2016). However, Liang and colleagues developed a DNA-free genome-editing system that writes-off the mRNA disadvantage (Liang *et al*., 2017;2018). The Cas9/sgRNA (ribonucleoprotein) RNPs was shown to be as effective as the plasmid-base system and with low off-target frequency. This is because RNP cleaves the target upon delivery without cellular transcription and translation.

This study intended to research the role played by the *NFκB* pathway on the HAART induced insulin resistance in CHO-IR cells using CRISP/Cas9 system.

1.8 AIM

This study aimed to elucidate the role of NFκB in the insulin resistance caused by antiretroviral drugs by knocking out the endogenous gene in CHO cells using CRISPR-Cas9 technology

1.9 OBJECTIVES

The objectives of this project were:

- To design guide RNA (gRNA) and primers; and insert gRNA into the pSPCas9(BB) plasmid prior transfection into CHO-IR cells
- To confirm the deletion of NFκB by screening CRISPR/Cas9-mediated mutants using Heteroduplex Mobility Assay and Western blots.

Chapter 2: Materials and Methods

2.1. Reagents

Unless stated otherwise, restriction enzymes used in this study were purchased from New England Biolabs (NEB) United State of America (USA). All chemical reagents were purchased from Merck, USA unless stated otherwise. *Escherichia coli* (*E. coli*) XL gold cells were a precious gift from Dr Iman van Den Bout from Physiology Department at the University of Pretoria. Unless stated otherwise, all amplifications were done using Labnet Multigene™ gradient thermocycler (Labnet International Inc., USA). The following antibodies were used in this study: α-NFκB1 p105 polyclonal mouse primary antibody, α-actin polyclonal mouse antibody and α-mouse polyclonal secondary antibody (Thermo Fisher Scientific, USA) (a precious gift from Mr Lutendo Mathomu from the Department of Biochemistry, BioNanoC research group, University of Venda). Both the MSc committee and Ethics group (346/2018) at the University of Pretoria approved the project.

2.2. gRNAs and Primers design

For the identification gRNAs, Synthego (http://design.synthego.com/#/, accessed on 15th of May 2018), an online tool was used. Upon opening the site, species and gene of interest were entered [*Cricetulus griseus* RefSeq: C_griseus_V1.0 (GCF_000419365.1) rel102 and NFκB1 Ref 100770607] respectively. Top 2 search results which target exon 6 from 118445 to 118593 bp were then selected and were used for the rest of the study. The hU6-F primer was obtained from the addgene website (https://www.addgene.org/browse/sequence/106034/). For other primers, Primer-BLAST and CLC Main Workbench by NCBI and Qiagen respectively were used for design. Briefly, https://www.ncbi.nlm.nih.gov/tools/primer-blast/ link was followed, and the plasmid sequence was entered. After searching, 5 top quality primers were selected and sent to Inqaba Biotech for synthesis. All oligonucleotides used in this study were synthesised from Inqaba Biotech. Tables 2.1 and 2.2 summarise all oligonucleotides and primers.

Table 2.1. Oligonucleotides used to make gRNA 1 and gRNA 2.

Oligonucleotide	Sequence (5'---3')	Restriction enzymes	Subcloning vector
CRISPR 1 *(Forward)*	AAACTTGGTGACCAATTGAACAATC	BbsI	pX330
CRISPR 2 *(Reverse)*	CACCGATTGTTCAATTGGTCACCAA	BbsI	
CRISPR 3 *(Forward)*	AAACTTGCAGGTCCCACATAGTTGC	BbsI	pX330
CRISPR 4 *(Reverse)*	CACCGCAACTATGTGGGACCTGCAA	BbsI	

Table 2.2. Primers used in this project.

Primers	Sequence (5'---3')
hU6-F *(forward)*	GAGGGCCTATTTCCCATGATT
R-OLIG_3 *(Reverse)*	CCAAGTGGGCAGTTTACCGT
Rev-1 *(Reverse)*	CTAAAAGCAGAACAGTGGG
Forw-1 *(forward)*	AGTTAGAGAGGGGCTGGA

2.3. Cell cultures

Both mammalian and bacterial cultures were used in this study, below is the brief methods used for culturing:

2.3.1 Bacterial cell culture

All bacterial cells were grown on either LB broth or LB agar (Sigma-Aldrich, Germany). For the preparation of the 10x media, 20.6 g of LB broth was mixed with 1L MilliQ water. The mixture was autoclaved for 20 minutes at 121 ˚C at 105 kPa of pressure using VCV autoclave (Sigma, USA). For agar plates formulation, 35 g of LB powder was mixed with 1l Milliq water. After autoclaving, just before media was ready for pouring, ampicilin at (50 ug/ml) was added . Finally, about 20 ml of media was then poured into respective 100 x 15 mm plates.

2.3.2 CHO-IR cell culture

Chinese Hamster Ovarian cell transfected with insulin receptors (CHO-IR) cells were cultured in Ham's F12 culture medium (Life Technologies, UK) in 75 cm^2 flasks, and incubated at 37 ˚C in a 5 % CO_2 incubator (Esco, Singapore). CHO-IR cells are ideal model for insulin signnaling owing to they ease to culture due to their short doubling time. They also have high level of insulin receptor protein expression, this play a crucial role in sensitivity detection of changes in signaling protein involved in the insulin signaling pathway.

The medium was supplemented with 10 % (v/v) fetal calf serum (FCS) (Life Technologies, UK), 10 % (v/v), 2 mM L-glutamine (Life Technologies, UK), and 100 U/ml penicillin, amphotericin and streptomycin (Life Technologies, UK), 0.5 % gentamicin and µg/ml G418-sulphate solution (Life Technologies, UK). Antibiotics and antimycotic were used to prevent common cell culture contamination, including bacterial and mycotic contamination. Gentamicin was used to prevent contamination of the mycoplasma in the cell medium. G418 is an antibiotic that ensures that only cells transfected with insulin receptor survive as compared to those without the plasmid.

Ham's F12 medium was used as a base medium for CHO-IR cells owing to its high level of L-proline, an amino acid required by the cell to grow. Foetal calf serum is enriched with insulin growth factor (IGF) which its primary function is to stimulate the growth of the cell. L-glutamine provides vital support in cellular growth, and serve as a substitute source of energy for rapidly dividing cells

After 3-4 day of culture, cells were split at 80 % cofluency for subculturing. Briefly, the culture medium was decanted out before rinsing cells with 10 ml phosphate-buffered saline (PBS) (Sigma Aldrich, USA). Then with 500 µl of 1X trypsin-ethylenedinitrilotetraacetic acid (Trypsin-EDTA) solution (Sigma Aldrich, USA). The flask was incubated at 37 ˚C for 2 minutes to allow cells to detach from the flask. The trypsinisation reaction was terminated with 5 ml of culture medium, and 1 ml of warm culture medium was transferred to a new flask containing 19 ml of new culture medium.

2.4. Plasmid DNA extraction

Plasmid DNA was extracted using two methods, depending on the intended use and throughput. Below is the brief methodology followed in each method:

2.4.1 Mini-prep

For small scale DNA extraction, ZymoPURE™ plasmid Miniprep kit (Zymo Research, USA) was used. Briefly, 5 ml of bacterial culture was centrifuged in a transparent 1.5 ml tube at maximum speed for 30 seconds in a microcentrifuge and supernatant was discarded. 250 µl of ZymoPURE™ P1 was added to the bacterial cell pellet and resuspended completely by vortexing. 250 µl of ZymoPURE™ P2 was added before immediate mixing by gently inverting the tube 8 times. The mixture was allowed to incubate at room temperature for 3 minutes until cells appeared transparent, purple, and viscous. 250 µl of ice-cold ZymoPURE™ P3 was added and mixed thoroughly by inversion until yellowish precipitate form. The neutralised lysate was then incubated on ice for 5 minutes. The neutralised lysate was centrifuged for 5 minutes at 16,000 x g.

A volume of 600 µl supernatant was transferred into a clean 1.5 ml microcentrifuge tube without disturbing the yellow pellet and avoiding transferring any cellular debris to the new tube. A volume of 275 µl ZymoPURE™ Binding Buffer was added to the cleared lysate and mixed thoroughly by inverting the capped tube 8 times. A Zymo-Spin™ II-P Column was placed in a Collection Tube, and the lysate was transferred into the Zymo-Spin™ II-P Column prior incubation the assembly at room temperature for 2 minutes and then centrifuged at 5,000 x g for 1 min. The flow-through was discarded. 800 µl of ZymoPURE™ Wash 1 was then added to the Zymo-Spin™ II-P Column and centrifuged at 5,000 x g for 1 min. The flow-through was discarded. Exactly 800 µl of ZymoPURE™ Wash 2 was added to the Zymo-Spin™ II-P Column and centrifuged at 5,000 x g for 1 min discarding the flow-through. 200 µl of ZymoPURE™ Wash 2 was added to the Zymo-Spin™ II-P Column and centrifuged at 5,000 x g for 1 min, discarding the flow-through. The Zymo-Spin™ II-P Column was centrifuged at 10,000 x g for 1 minute in order to remove any residual wash buffer. The Zymo-Spin™ II-P Column was then transferred into a clean 1.5 ml tube, and 25 µl of ZymoPURE™ Elution Buffer was added directly to the column matrix and incubated at room temperature for 2 minutes, and then centrifuged at 10,000 x g for 1 minute in a microcentrifuge. Eluted plasmid DNA was stored at -20°C until further use.

2.4.2. Midi-prep

For the extraction of plasmid DNA in large quantities, ZymoPURE™ II plasmid Midprep kit (Zymo Research, USA) was used. Briefly, 50 ml overnight culture was centrifuged to remove media at 10,000 RPM for 5 minutes. A volume of 8 ml ZymoPURE™ P1 was added to the bacterial cell pellet and resuspended completely by vortexing. 8 ml of ZymoPURE™ P2 was added prior to a rapid mixing by gently inverting the tube 6 times. The mixture was allowed to sit at room temperature for 3 minutes until the mixture turns purple. 8 ml of ZymoPURE™ P3 was added and mixed gently but thoroughly by inversion until the mixture turns yellow.

Plugs were attached to the Luer Lock at the bottom of the ZymoPURE™ Syringe Filter and placed upright in a tube rack and lysates were loaded into the ZymoPURE™ Syringe Filter and waited for 8 minutes for the precipitate to float to the top. The Luer Lock plug was removed from the bottom of the syringe and placed into a clean 50 ml conical tube. Plunger was placed in the syringe and solution was pushed through the ZymoPURE™ Syringe Filter in one continuous motion until approximately 20 ml of cleared lysate was recovered. The cleared lysate was saved. 8 ml of ZymoPURE™ Binding Buffer was added to the cleared lysates and mixed thoroughly by inverting the capped tube 8 times. A 50 ml Reservoir was removed from the top of the Zymo-Spin™ III-P Column Assembly, and the 15 ml Conical Reservoir and Zymo-Spin™ III-P column were connected and placed into a 50 ml conical tube.

A 10 ml of the mixture was added into the 15 ml Conical Reservoir/ZymoSpin™ III-P Column assembly and centrifuged at 500 x g for 2 minutes. The 50 ml conical tube was emptied, and this step was repeated until the entire sample has passed through the column. 2 ml of ZymoPURE™ Wash 1 was added to the Zymo-Spin™ III-P column assembly and centrifuged at 500 x g for 2 minutes. 2 ml of ZymoPURE™ Wash 2 was added to the Zymo-Spin™ III-P column assembly and centrifuged for 2 minutes at 500 x g. For the removal of all impurities, this step was repeated. The purple Luer Lock cap was unscrewed from the top of the Zymo-Spin™ III-P Column and the 15 ml Conical Reservoir was discarded. The Zymo-Spin™ III-P Column was placed in a Collection Tube and centrifuged at 10,000 x g for 1 minute, in a microcentrifuge, to remove any residual wash buffer. The column was transferred into a clean 1.5 ml microcentrifuge tube. Subsequently, 200 µl of ZymoPURE™ Elution Buffer was added directly

to the column matrix after waiting for 2 minutes, and then centrifuged at 10,000 x g for 1 minute in a microcentrifuge. Eluted DNA was stored at -20°C until further use.

2.5. Agarose gel electrophoresis

A 0.8 % agarose tablet was dissolved in 1x TAE buffer (40 mM Tris, 20 mM acetic acid and 1 mM EDTA) by microwaving. The agarose was cooled to 55 °C before adding ethidium bromide (0.5 µg/ml). The agarose gel was then allowed to polymerise for 15-30 minutes at room temperature. The gel was then placed in the electrophoresis chamber and covered with 1x TAE buffer. A volume of 4 µl of 10x DNA loading buffer (0.25 % bromophenol blue, 30 % glycerol) was added to 20 µl of the sample followed by loading the samples into the wells. Electrophoresis was run at 100 volts for 1 hour using Labnet Enduro power supplier 300v (Labnet International Inc, USA).

2.6. Restriction digest

Plasmid DNA was confirmed by restriction digestion. Three autoclaved tubes were labelled A, B and C, and samples containing pX330-U6-Chimeric_BB-hSpCas9 (plasmid #42230, Addgene), pSpCas9(BB)-2A-GFP (pX458) (plasmid #48138, Addgene) and pSpCas9(BB)-2A-Puro(pX459) (plasmid #62988, Addgene) were added in each tube, respectively. In tube A, and B 3 µl of EcoRI-HF (20000 units/ml), EcoRV-HF (20000 units/ml) and 10X NEBuffer and topped up-to 50 µl with dH_2O. In tube C, 3 µl of EcoRI-HF (20000 units/ml), EcoRV-HF (20000 units/ml), StuI (10000 units/ml) and 10X NEBuffer and topped up-to 50 µl with dH_2O. The reaction mixtures were then incubated in 37 ˚C water bath for 11 minutes. Reactions were then inactivated by incubating at 65 ˚C for 20 minutes before the addition of 10 µl of 6X gel loading dye provided with restriction enzymes. Results were resolved on a 0.8 % (w/v) agarose gel.

Table 2.3. Summary of the restriction digest reaction for plasmid DNA conformation.

Reagent	pX330	pX458	pX459
EcoRI (µL)	3	3	3
EcoRV (µL)	3	3	3
StuI (µL)	-	-	3
10x NEBuffer	3	3	3
RNAse free water (µL)	33	31	29
DNA (µL)	8	10	9
Total (µL)	50	50	50

For the preparation for ligation, 3µL of 50 ng pX330-U6-Chimeric_BB-hSpCas9 (plasmid #42230, Addgene), 1 µL of 20000 units/ml BbsI-HF restriction enzyme, 3 µL of 10x NEBuffer, 23 µL nuclease-free water was added in a tube and briefly mixed. The mixture was incubated 10 minutes at 37 °C and followed by incubation at 65 °C for 20 minutes in VCBV incubator (Bio-Rad, USA). A volume of 6 µL of loading dye was added on the mixture to stop the reaction. The mixture was then run on 0.5 % (w/v) agarose gel at 100 volts for 1 hour using Labnet Enduro power supplier 300v (Labnet International Inc, USA) and visualised using Uvitec FireReader V10 Imaging system (BioSPX, Netherlands).

2.7. Gel extraction

Gel extraction was performed using QIAquick Gel extraction kit (Qiagen, USA) by following the manufacturer's protocol. In brief, after agarose gel electrophoresis, the gel was excised with a sharp, clean surgical blade on a Uvitec FireReader V10 Imaging system (BioSPX, Netherlands) and weighed out in a clean colourless tube. A 3 X volume of buffer QC was added to 1X gel volume provided that 1000 mg gel equates to 100 mL. The mixture was incubated in 50 °C for 10 minutes with brief mixing by vortex in 3 minutes intervals until the gel was completely dissolved. Then 1 volume of isopropanol was added to the sample and mixed. The mixture was then transferred into a column. The column was then placed into 2 mL collection tube and spun down for 1 minute at 13000 rpm.

The flow-through was later discarded. Then, 750 µl of buffer PE was added into the membrane and was centrifuged at 13000 rpm for 1 minute after it was incubated for 5 minutes at room temperature to wash residues in the membrane. The flow-through was discarded before the tube was transferred to a new clean collection tube. Then, 30 µL of elution buffer was added

and was incubated for 1 minute at room temperature before spinning down at 13000 rpm for 30 seconds. Eluted DNA was then stored at -20 °C until further use.

2.8. Dephosphorylation of vector DNA and annealing of primer pairs

Dephosphorylation was performed to ensure that vector DNA did not re-circularize during ligation. Limiting re-circularization reduces background during the subsequent transformation (Ukai *et al.,* 2002). Shrimp alkaline phosphatase (rSAP) (New England Biolabs Inc, USA) was used following manufacture's protocol. Briefly, 1 pmol of px330 digested plasmid DNA (5 µl), 2 µl of 10x CutSmart® buffer, 2 µl of 1000 units/ml rSAP and 11 µl of distilled water as added in a clean 0.2 ml tube. The mixture was then incubated at 37 ˚C water bath for 30 minutes. The mixture was subjected to heat-inactivation to stop the reaction by incubation at 65 ˚C in a heating block for 5 minutes.

Annealing of reverse and forward primer was performed to get complementary oligonucleotides. Protocol from a Ran *et al.,* 2013 was used for this purpose with some modifications where required CRISPR 1 and CRISPR 2 primers were used to make gRNA 1, and CRISPR 3 and CRISPR 4 were used to make gRNA 2. In an Eppendorf tube, the components were mixed in a proportion as summarized in a table below:

Table 2.4. Composition of gRNA 1 and annealing.

Reagent (gRNA 1)	Volume (µL) [concentration (µM)]
CRISPR 1 *(Forward)*	1 [5]
CRISPR 2 *(Reverse)*	1[5]
10 X ligation buffer	1[1X]
RNAse free water	6.5
T4 NPK	0.5 [5units]
Total	10

Table 2.5. Composition of gRNA 2 and annealing.

Reagent (gRNA 2)	Volume (µL) [concentration (µM)]
CRISPR 3 *(Forward)*	1 [5]
CRISPR 4 *(Reverse)*	1[5]
10 X ligation buffer	1[1X]
RNAse free water	6.5
T4 NPK	0.5 [5units]
Total	10

The mixture was ran in a thermocycler as shown in Table 2.6 below using Labnet Multigene™ gradient thermocycler TC9600-G (Labnet International Inc., USA)

Table 2.6. Cycling conditions for oligonucleotide annealing.

Step	Temperature ˚C	Time (minutes)
Hold	37	30
Hold	95	5
Ramp down	*	*

*ramped down to 25 ˚C at 5 ˚C/min

2.9. Ligation

Ligation was performed to join the annealed pair of primers to the digested pX330-U6-Chimeric_BB-CBh-hSpCas9 (Addgene plasmid #42230). The reaction was set as summarised a table below:

Table 2.7. Composition of gRNAs ligation to the plasmid.

Reagent	Volume	concentration
BbsI digested plasmid	2	40 unit/µl
Annealed gRNA	1	40 ng
10x T4 DNA ligase buffer	5	2x
RNAse water	2	-
Ligase	1	1x
Total	10	-

The reaction mixture was then incubated at room temperature for 10 minutes. Ligated plasmids were then transformed into XL10 Gold *E. coli, as* explained in the next subsection.

2.10. Competent cells

Single colonies of *E. coli* XL10 gold {Tet^r *Δ*(*mcrA)183* Δ(*mcrCB-hsdSMR-mrr*)*173 endA1 supE44 thi-1 recA1 gyrA96 relA1 lac* Hte [F′ *proAB lacI^{q}ZΔM15* Tn*10* (Tet^r) Amy Cam^r]} was inoculated into 5 ml 10x LB broth (Sigma-Aldrich, USA) and grown for overnight at 37 °C with shaking (150 rpm). The overnight culture was diluted into 1:10 fresh 10X LB broth and thereafter grown with shaking to early log phase of absorbance 0.3-0.5 measured at 600 nm wavelength by spectrophotometry (Bio-Rad, USA). Cells were harvested by centrifuging at 5,000 rpm for 10 minutes at 4 °C. Cells were then kept on ice from this point onwards. The supernatant was then discarded before the pellets were resuspended with ice-cold transformation storage solution (TSS) buffer (0.0125 M PEG, 0.03 M $MgCl_2$, 5 % DMSO, 10X LB broth) by a vortex. Cells were then aliquoted into tubes and stored at -80 °C till further use.

2.11. Transformation

The transformation experiment was performed to amplify and store ligated plasmid. In 3 Eppendorf tubes, 100 µL of chemical competent XL10 Gold cells were placed on each. Then 2 µL of ligated plasmids were placed on one tube, 2 µL of original plasmid was added on another tube to serve as a positive control, and 2 µL of water was added on the other to serve as a negative control. The mixture was left to chill on ice for 30 minutes before being heat shocked for 45 seconds at 42 ˚C heating block (Bio-Rad, USA). Samples were then again chilled in ice for 10 minutes before addition of chilled 10 X LB broth.

The mixture was then incubated for 1 hour at 37 ˚C shaking incubator rotating at 250 rpm (Labnet International Inc, USA). After incubation, 100 µL from each tube was streaked on LB agar plates as dilute samples. The remainder was subjected to centrifugation at 10,000 rpm at 4 ˚C for 5 minutes. After centrifugation, 800 µL of supernatant was discarded, and the remaining supernatant was then mixed with pellets fraction before plating to LB agar plate as a concentrated sample. Plates were incubated overnight at 37 ˚C on Labnet 211DS shaking incubator (Labnet International Inc, USA).

2.12. Colony PCR

Cloning success was detected by colony PCR. Briefly, colonies were tested with PCR using Quick-Load® Taq 2X Master Mix (New England Biotech, USA). Shortly, a 50 µl reaction was set up consisting of 25 µl Quick-Load® Taq 2X Master Mix (1X), 3 µl each of the hU6-F and R-OLIG_3 primer (50 µM), and PCR water to 50 µl as summarized in a table below. A sterile toothpick was used to pick up an individual colony and dipped into each reaction tube. Each toothpick was then dipped into 3 ml of growth media to create a particular stock.

The mixture was subjected to amplification in using parameters stipulated in table 2.8. A Labnet Multigene™ gradient thermocycler (Labnet International Inc., USA) was used for this reaction. PCR products were analysed by agarose gel electrophoresis as described previously (section 2.10) and visualised using Uvitec FireReader V10 Imaging system (BioSPX, Netherlands).

Table 2.8. Thermocycling conditions used to amplify plasmid DNA from colonies

Step	Temperature(°C)	Time	Cycles
Hold	94	30 s	
Denaturation	94	15 s	
Annealing	65	15 s	30
Extension	68	30 s	
Incubation	68	5 mins	
Maintenance	4	∞	

2.13. PCR

The polymerase chain reaction was performed using Quick-Load® Taq 2X Master Mix (New England Biotech, USA). Briefly, a 25 µl reaction was set up consisting of 12.5 µl Quick-Load® Taq 2X Master Mix (1X), 0.5 µl each of the CRISPR 1/ CRISPR 3 and R-OLIG_3 primer (1 µM), and PCR water to 25 µl (concentration as suggested by supplier). PCR was run using conditions as detailed in Table 2.9, using Labnet Multigene™ gradient thermocycler (Labnet International Inc., USA). Amplicons were analysed by agarose gel electrophoresis as described previously (section 2.10) and visualised using Uvitec FireReader V10 Imaging system (BioSPX, Netherlands).

Table 2.9. Thermocycling conditions used to amplify extracted plasmid DNA from colonies.

Step	Temperature(°C)	Time	Cycles
Hold	94	30 s	
Denaturation	94	15 s	
Annealing	65	15 s	30
Extension	68	30 s	
Incubation	68	5 mins	
Maintenance	4	∞	

2.14. Sanger sequencing

From PCR results, positive clones were sequenced, and chromatogram results were then sent and analysed with SnapGene® (GSL Biotech LLC, USA). Sanger sequencing relies on chain termination method. This is achieved by performing PCR mehod with inclusion of dideoxynucleotides (ddNTPs) whose ribose lack hydroxyl groups in position 2' and 3'. (Munshi 2012, p. 6) Lack of these hydroxyl groups terminates the reaction, and nucleotide in that position is determined. This is achieved by labelling ddNTPs with different wavelengths of fluorescence and emissions (Munshi 2012, p. 6).

2.15. Calcium phosphate transfection.

Six hours before transfection, 2.25 ml of 0.5 x 10^5 cells were transferred in 500 µl of growth medium without antibiotics till they reach 80 % confluent. For the transfection, cells were split by transferring 2.25 ml into each of the 6-well plates. Plasmid DNA was prepared for transfection. Preparation for each well was done as outlined, 5 µg of plasmid DNA was mixed with 16 µl of 2M $CaCl_2$ and topped up to 125 µl of ddH_2O before thorough mixing in a sterile tube. The DNA-$CaCl_2$ mixture was then mixed with 125 µl of 2X HBS [280 mM $NaCl_2$; 10 mM KCl; 1.5 mM $Na_2HPO_4.H_2O$; 12 mM dextrose (glucose); 50 mM HEPES pH 7.05; filter sterilised with 0.22 µl filter]. The DNA/$CaCl_2$/HBS mixture was incubated at room temperature for 30 minutes before thorough mixing again. The mixture was then sprinkled entirely in a well. Cells were transferred to an incubator at 37 ˚C and 5 % CO_2 for overnight. Following morning, plates were gently swirled, and the medium was later discarded. Then 2.5 ml of fresh medium with puromycin for selection of successfully transfected cells were added and incubated at 37 ˚C,

and 5 % CO_2 and cell growth were monitored in a daily basis with a simple microscope(Zeiss, Germany).

2.16. Flow cytometry

A specialised flow cytometry was used to sort heterogenous mixture of cells into wells, one cell at a time. This is achieved by subjecting cells in a centre of narrow and rapid flowing fluid. A vibrating mechanism cause liquid to break into droplets. A charge is placed on the ring based immediately before florescence meter and opposite charge is trapped and same charge passes to the container.

The cell populations were subjected to sorting to achieve one cell per well. Briefly, cells were harvested by treating with trypsin and incubation at 37 ˚C for 10 minutes as explained before.. Cells were collected and transported to the Institute for Cellular and Molecular Medicine (ICMM), at the University of Pretoria in a polystyrene container. Cells were sorted by BD FacsAria Fusion using BD FACSDiva Software version 8.0.1, nozzle size (70 micron) single cell mode. Cells were collected on a 96-well plate with 50 µl. Tey were then transported back to the lab and nurtured in incubator (Esco, Singapore) at 37 ˚C in a 5 % CO_2.

2.17. Genomic DNA isolation

Genomic DNA was isolated using *Quick*-DNA™ Miniprep Plus Kit (Zymo Research, USA) with minor modifications. Briefly, cells were trypsinized from flask using trypsin treatment, as explained before. Cells were spun down at 500g for 2 minutes. Pellets were then resuspended with 200 µl of elution buffer before the addition of 200 lysis buffer and 20 µl Protease K solution and vortexed thoroughly for 15 seconds before incubation at 55 ˚C for 10 minutes. Then the mixture was transferred to a Zymo-Spin™ IIC-XLR Column in a Collection Tube and centrifuged at 12,000 x g for 1 minute. Collection tube with the flow-through was discarded.

400 µl DNA Pre-Wash Buffer was added to the spin column in a new Collection Tube and centrifuge at 12,000 x g for 1 minute before emptying the collection tube. 700 µl g-DNA Wash Buffer was added to the spin column and spun down 12,000 x g for 1 minute. 200 µl g-DNA Wash Buffer was added to the spin column and centrifuge at 12,000 x g for 1 minute before discarding the collection tube with the flow-through. The spin column was transferred to a

clean microcentrifuge tube. 50 µl DNA Elution Buffer was added directly on the matrix and incubated for 5 minutes at room temperature, then centrifuged at maximum speed for 1 minute to elute the DNA was stored at -20 ˚C for future use.

2.18. Mixing heteroduplex mobility assay

In order to determine the success of CRISPR/Cas9, a mixing heteroduplex assay (mHMA) was used as described in Foster *et al* (2018). Briefly, genomic DNA (gDNA) was extracted using Zymo genomic DNA extraction kit (USA), and PCR was performed as described in section 2.15 above using Forw-1 and Rev-1 primers. The amplicons were subjected to denaturation at 95 ˚C and were allowed to reach room temperature on the benchtop for slow renaturation of amplicons to form heteroduplexes.

The mixture was run in 8 % tris-borate-EDTA (TBE) polyacrylamide gel [15 % Acrylamide-Bisacrylamide(29:1) 5 X TBE, 10 % APS, 10 % TEMED] with 1 X TBE running buffer (1.1 M tris base, 1.1 M boric acid, 0.2 M EDTA) as described by Zhu *et al* 2014 . 2 µl of the sample were loaded and ran for an hour at 150 V. The gel was then soaked in 0.5 µg/ml of ethidium bromide (EtBr) for 10 minutes before viewing in Uvitec FireReader V10 Imaging system (BioSPX, Netherlands).

In order to distinguish homozygous mutants from homozygous wild type, mHMA was performed. Briefly, amplicons from the identified homozygous bands were mixed in a 1:1 ratio with amplicons from a known wild type and denatured before renaturation as described above. After resolving the gel, the results from the first round and identify homozygous mutant by determining the amplicons that follow the heterozygous patterns.

Table 2.10. Thermocycling conditions used to amplify extracted CHO-IR DNA.

Step	Temperature(°C)	Time	Cycles
Hold	94	30 s	
Denaturation	94	15 s	
Annealing	57	15 s	30
Extension	68	30 s	
Incubation	68	5 mins	
Maintenance	4	∞	

2.19. Western blots

Western blot analysis was performed to confirm the gene knockout. Proteins were isolated from cells using in-house lysis buffer. Briefly, cells were harvested as explained before and placed in a 1.5 ml tube. Subsequently, 100 µl lysis buffer [50 mM 4-(2-hydroxyethyl)-1-piperazineethanesulfonic acid (HEPES), pH 7.5, 1 % phenoxylpolyethoxyethanol (NP40), 10 % glycerol, 50 mM sodium chloride (NaCl), protease inhibitor cocktail tablet (PICT)(Merck, USA) and phosphatase inhibitor (Merck, USA)] was added evenly to the tubes, which were placed ice for 10 min. Protease (Roche, Switzerland) and phosphatase inhibitors (Roche, Switzerland) were added to the lysis buffer to serve a protective role to cellular proteins against dephosphorylation. Protease inhibitor in particular, inhibits a wide range of proteases from metalloproteases to calpains. In contrast, phosphatase inhibitor inhibits a range of phosphatases such as serine/threonine and tyrosine-protein phosphatase.

The cells were subsequently centrifuged at 4 °C at 10 000 rpm for 10 min. A volume of 60 µl cells was well mixed with 15 µl of 5 x Laemmli buffer (25 nM Tris, pH 6.8, 2 % SDS, 0.002 % bromophenol blue, 10 % glycerol and 5 % 2-mercaptoethanol) before boiling at 100 °C for 5 min, and brief spinning to settle all the evaporation from the lid of the microcentrifuge tube. The cell lysate was stored at -20 °C for short-term use or at -80 °C for extended storage.

Western blots were carried out as follows; proteins were separated with 12 % SDS-PAGE. The proteins were subsequently transferred onto a nitrocellulose membrane (Bio-Rad, USA) in Western transfer buffer [25 mM Tris, 192 mM glycine, 20 % (v/v) Methanol] for 1 hour at 10 volts using Bio-Rad TransBlotter. Blot was then stained with Ponceau-S stain [0.1 % (w/v) Ponceau-S in 5 % (v/v) acetic acid] to determine the success of the transfer. Ponceau stain was then washed off with TBS buffer. The membrane was then immersed in blocking solution [5 % non-fat milk prepared in TBST (50mM Tris, 150 mM NaCl, 0.1 % Tween-20)] for 1 hour shaking at 50 rpm. The membrane was then washed 3 times in 15 minutes intervals with TBST followed by incubation with anti-NFκB primary mouse antibody in blocking solution at 4 ˚C for 1 hour. Unbound antibodies were removed by washing the membrane 3 times with TBST for 15 minutes per wash. Afterwards, the membranes were immersed in secondary anti-mouse antibodies for 1 hour at 4 °C. Unbound antibodies were removed by washing the membrane 3 times with TBST for 15 minutes per wash. Bands were then visualised using enhanced

chemiluminescence (ECL) developing reagent (Bio-Rad, USA) and visualisation was done using Chemidoc ™ MP imaging system (Bio-Rad, USA).

Chapter 3: Results

3.1. gRNA and off-target

Synthego (https://www.synthego.com/products/bioinformatics/crispr-design-tool, accessed, on 15th May 2018) was utilised to determine and select proper gRNA for this project. This was done to ascertain that proper gRNA was used to knock-out the gene of interest, NFκB1. The gene knock out is illustrated below (Figure 3). In Figures 3.1 gRNA sequences, PAM and site of DSB are shown a) and the mismatch score b) for the two determined gRNA 1.

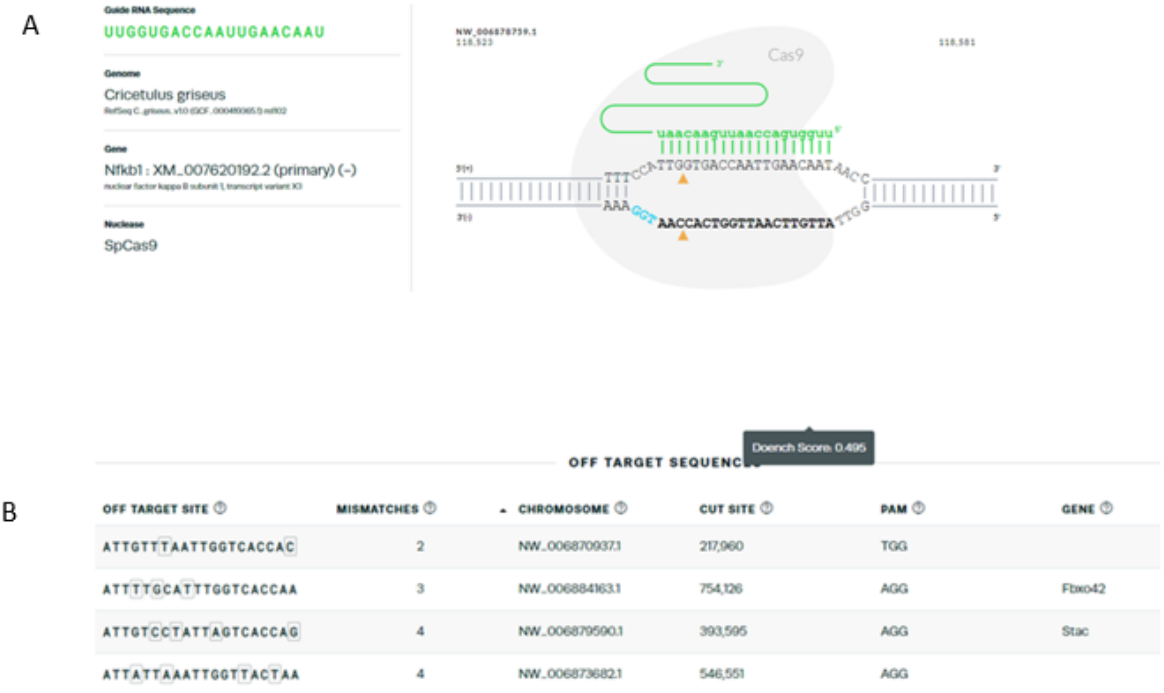

Figure 3.1. A) gRNA sequence gRNA 1 showing the recognition site and location where the DBS will occur and B) the off-target score b).

In Figures 3.2 gRNA sequences, PAM and site of DSB are shown a) and the mismatch score b) for the two determined gRNA 2. gRNA 2 showed a little off target as compared to gRNA 1 with

a mismatch score of 2. Both sequences showed to target the forward strand and induce DSB at 118,533 and 118,548 base pair respectively.

A

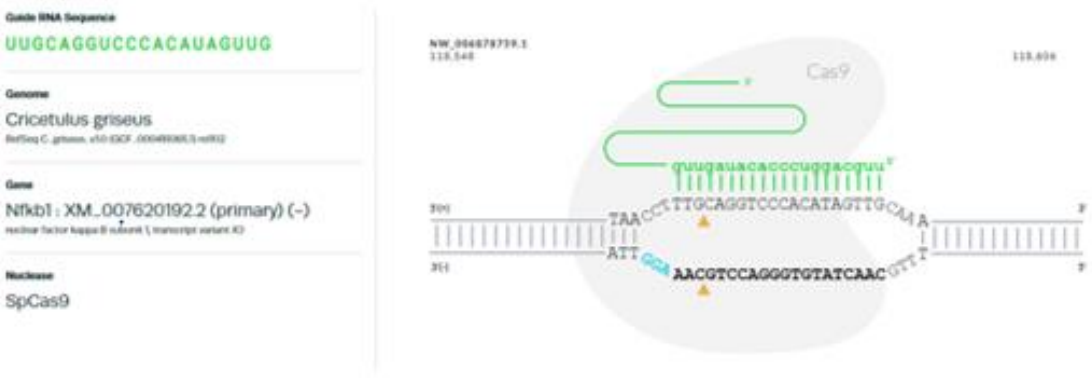

B

OFF TARGET SEQUENCES

OFF TARGET SITE	MISMATCHES	CHROMOSOME	CUT SITE	PAM	GENE
CAACTATGTGGGACCTGCAA	0	NW_006878759.1	118,572	AGG	Nfkb1
CCACCATGTGGGTCCTGCAA	3	NW_006879651.1	592,635	TGG	
CAACTGTGTGGGTCCTGCAT	3	NW_006884546.1	2,907,770	CGG	
AAACTGTGTGGCACCTGCAA	3	NW_006879066.1	845,793	TGG	Myo10
CAACTCTGTAGGTCCTGCAA	3	NW_006883214.1	672,855	TGG	
CAACTATGTGGGAACTTAGA	4	NW_006885753.1	2,737,427	TGG	

Figure 3.2 A) gRNA sequence gRNA 2 showing the recognition site and location where the DBS will occur and B) the off-target score.

3.2. Confirmation of recombinant plasmid DNA by restriction digest

The integrity of the plasmid was confirmed by restriction enzyme digestion and DNA resolved by 0.8 % agarose gel electrophoresis (Figure 3.3). In both gels, lane MW is molecular weight marker; lane 1 is PX330-U6_BB-CBh-hSpCas9 plasmid digested by *EcoRI* and *EcoRV* giving rise to two bands at 6204 bp and 2302 bp, respectively. Lane 2 is pSpcas9(BB)-2A-GFP (PX458) plasmid digested by *EcoRI* and *EcoRV* to give rise to bands at 6206 bp, 2299 bp and 783 bp

respectively. Lastly, in lane 3 is pSpcas9(BB)-2A-Puro (PX459) digested by *EcoRI, EcoRV* and *StuI* to give rise to bands at 6206 bp, 2299 bp, 400 bp and 269 bp respectively.

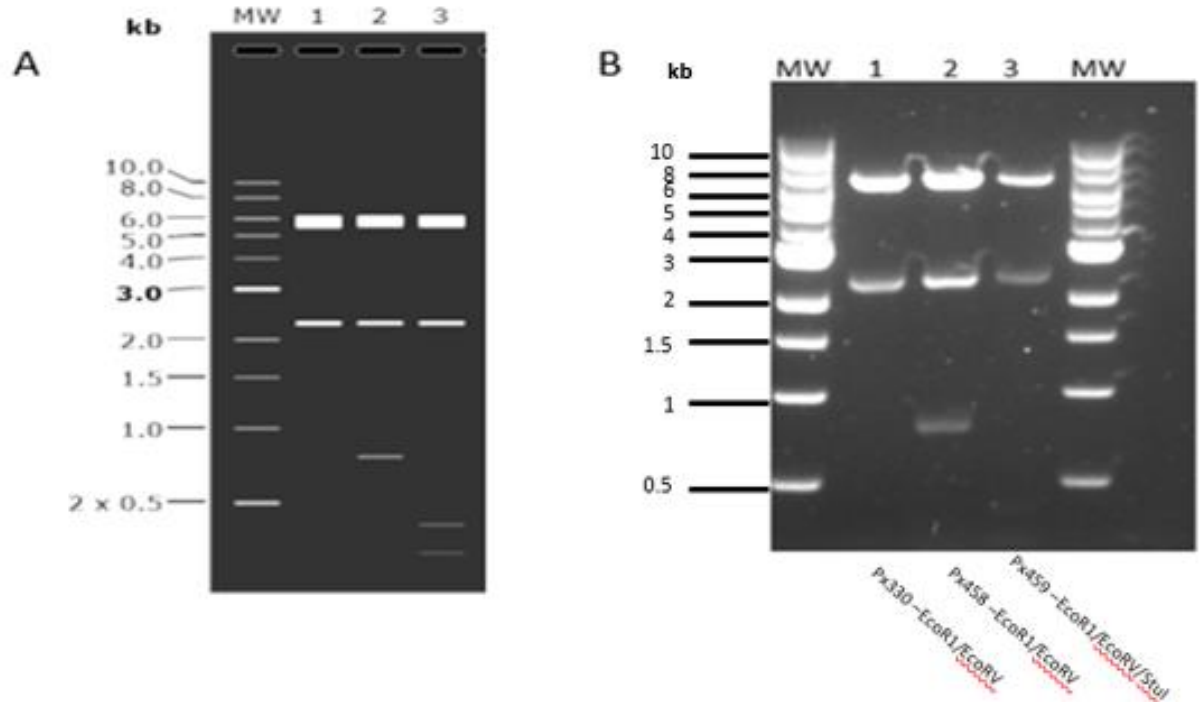

Figure 3.3. A: A gel simulation of restriction digest B: *In lane MW is a 1 kb DNA ladder, lane 1, px330 plasmid digested by EcoRI and EcoRV, lane 2 is PX458 plasmid digested by EcoRI and EcoRV; and lane 3 is PX459 digested by EcoRI, EcoRV and StuI.* Using 50 bp molecular marker (NEB)

3.3. Confirmation of ligation of plasmid and guide RNA oligonucleotides by PCR

After performing ligation of the gRNA into pX330 plasmid, plasmids were transformed into XL 10 gold competent cells, and they were subsequently plated on 2 X LB agar plates. Seventeen colonies grew from ligation of gRNA1, and 12 colonies grew from gRNA2. Subsequently, colony PCR was performed to confirm the success of ligation. Figure 3.4 below shows a 2 % agarose gel of the subsequent amplicons. Figure 3.4 a) and c) shows a simulation gel of the expected amplicon sizes b) and shows ligation of gRNA1 and d) that of gRNA2. In Figure 3.4a) and d) lane 1 is a positive control, lane 2 and 3 are the expected bands of the amplicon using the respective primers. In Figure 3.4. b) and d) lane MW is molecular weight marker, lane NTC is the non-

template control, lane -ve is the non-ligated plasmid control, lane +ve is a positive control, lanes 1-17 are colonies of gRNA1 and lanes 18-29 is colonies of gRNA2. As shown in Figure 3.4, the ligated clones presented a band at 333 bp, which was the expected band size. This observation confirms that the ligation was successful. Figure 3.5 shows the plasmid map for both gRNA 1 and gRNA 2 after ligation and the location of primers.

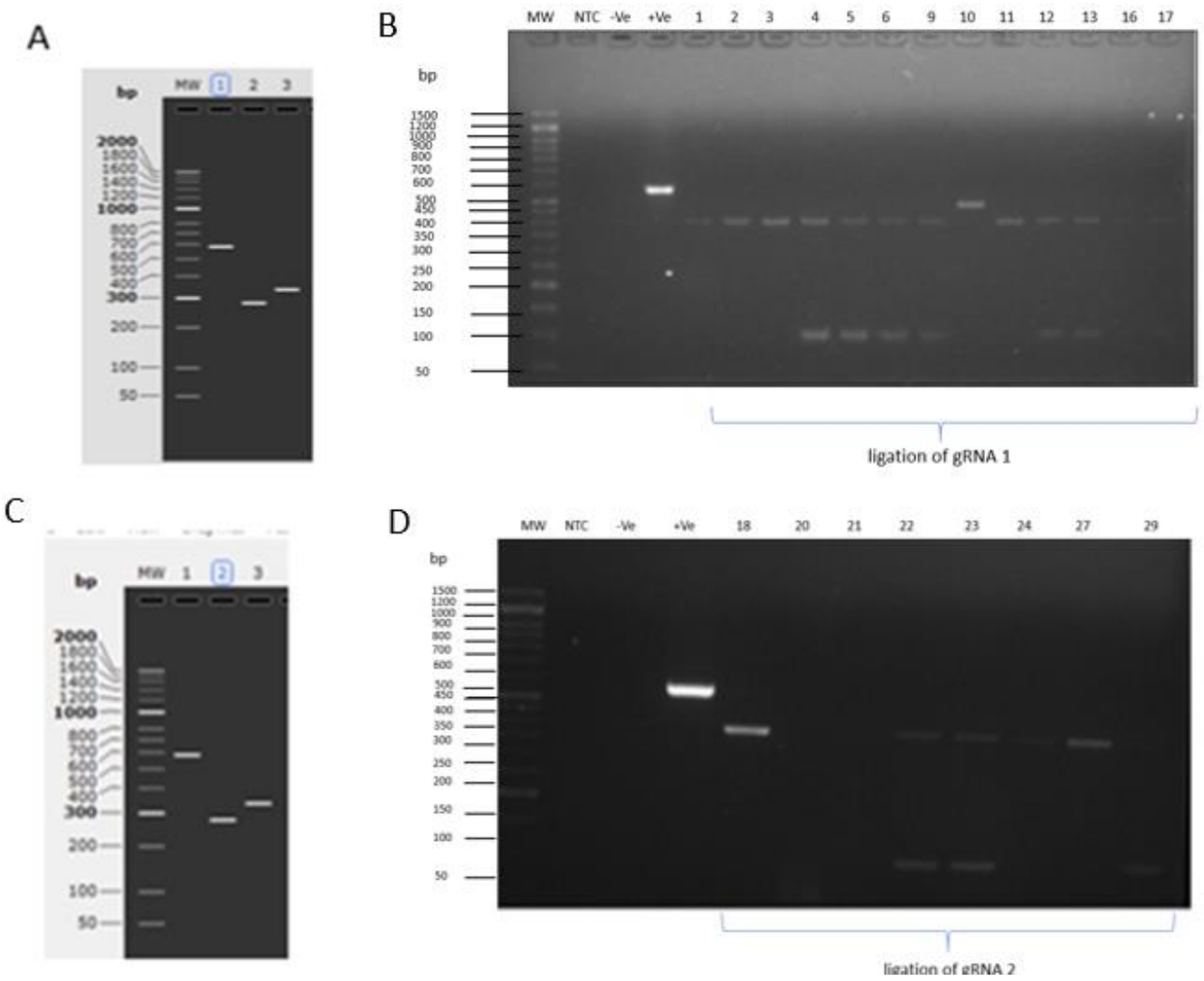

Figure 3.4. A gel simulation of PCR amplicon a) and c), and the actual agarose gel of the amplicons b) and d). In b) and d) lanes MW is molecular weight, NTC is the non-template control, -ve is the negative control, +ve is a positive control, 1-17 amplicons of gRNA 1 and 18-29 is amplicon of gRNA 2.

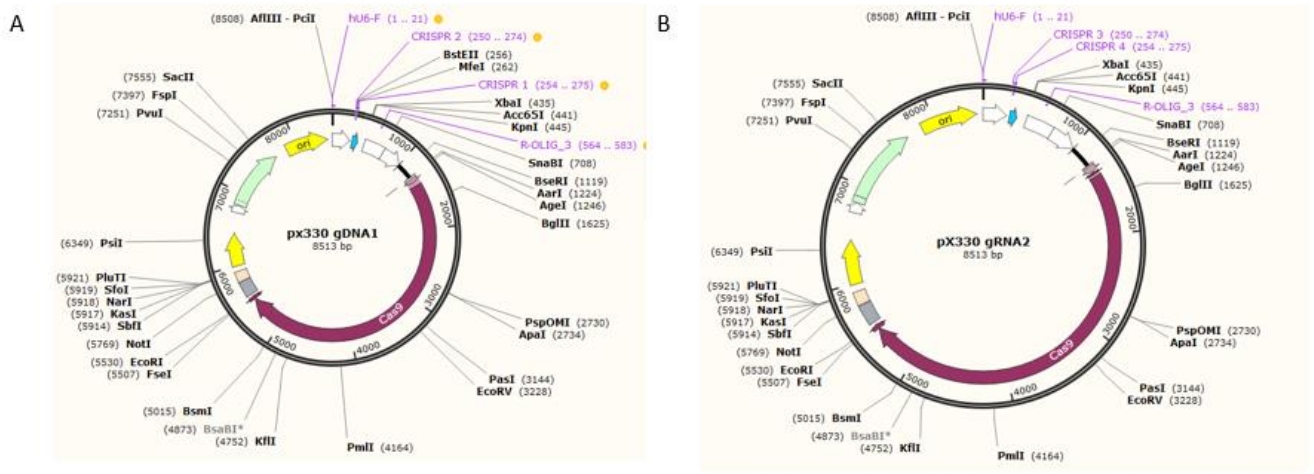

Figure 3.5. A plasmid map of pX330 plasmid after ligation with both gRNA 1 a) and gRNA 2 b) showing the insert, primers and restriction sites.

3.4. Confirmation of ligation of plasmid and guide RNA oligonucleotides by sequencing

In order to further confirm the ligation results, samples were sequenced using hU6-F and R-OLIG_3 primers. Three samples from each gRNA were analyzed. Sample 10 was included in Sanger sequencing to determine why its amplicon is of higher molecular weight than the rest. Figure 3.6, a) shows samples 3, 4 and 10 from ligation of gRNA1, b) shows samples 18, 23 and 27 from the ligation of gRNA2, c) and d) shows their respective chromatograms. Respective ligated gRNAs are highlighted in blue. The results further confirm that the ligation was successful as the expected sequence was found in clone 3 and 23 for gRNA 1 and gRNA 2, respectively. These two clones were then used for transfection.

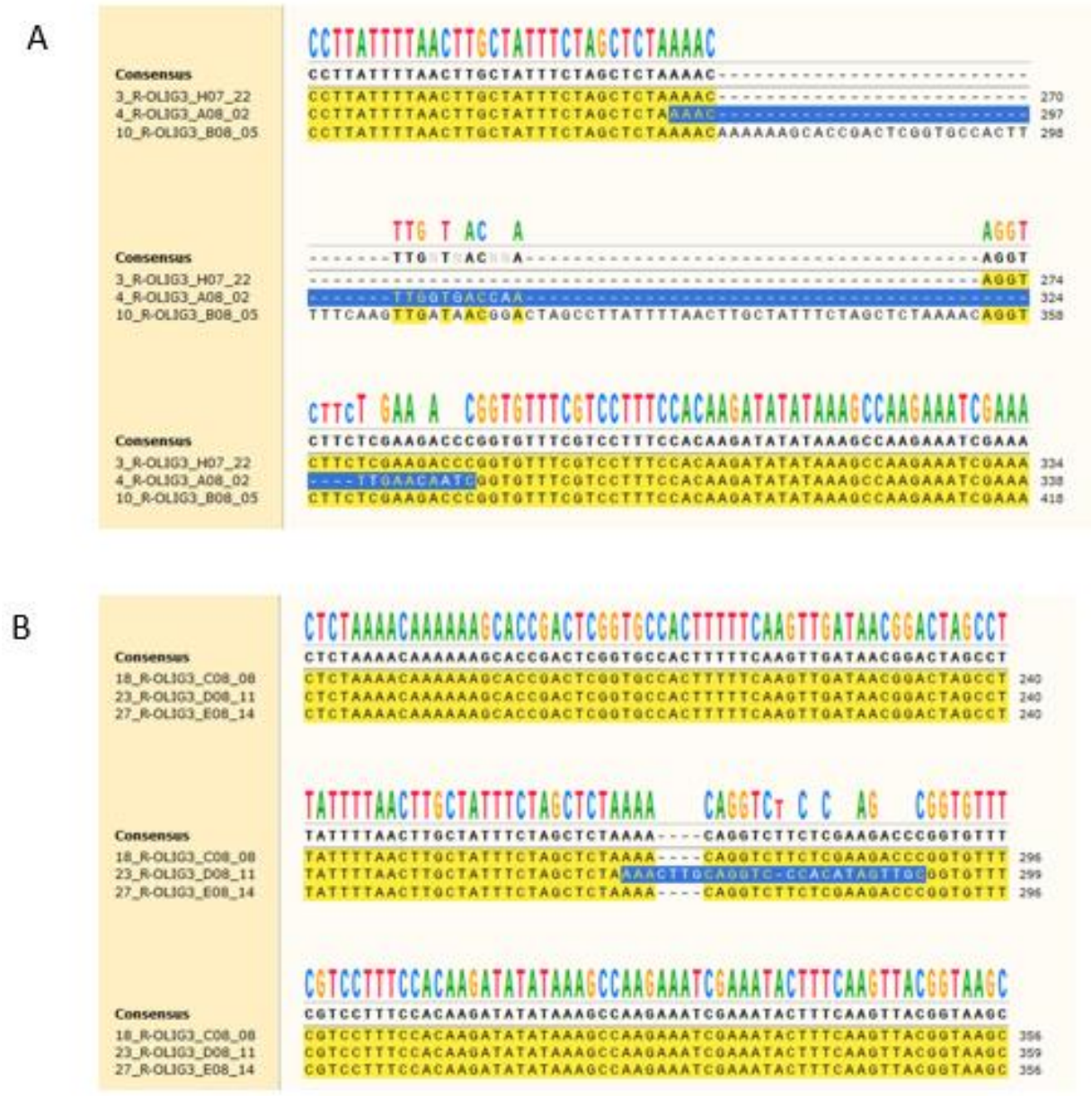

Figure 3.6. sequence results of plasmid pX330 after ligation with gRNA 1 a) and gRNA 2 b). sequence highlighted in blue shows the insert.

3.5. FACS

In order to obtain a single cell after transfection and then expand this, we passed the cell suspension through a fluorescent activated cell sorter (FACS Aria, Becton Dickinson) to separate GFP negative (GFP-) and GFP positive (GFP+) fractions, which were collected. The GFP was used as a marker protein, to trace and determine if transfection was successful. The sorting was performed at 70-micron nozzle size at room temperature. An illustration of those settings

is shown in figure 3.7. The left plot was used to sort cells according to cell size (forward scatter, FSC-A) vs granularity (side scatter, SSC-A) to exclude cellular debris as well as clumps of cells that may give erroneous fluorescent readings. A table on each shows the number of cells and percentage passed on the GFP gate as compared to all gates. GFP background was also compared to the control cells. Cells were only sorted according to the absence/presence of a fluorescent signal and not according to their viability. A) were control cells transfected with the non-ligated plasmid, B) and C) were cells transfected with gRNA 1 and gRNA 2-ligated plasmid respectively and D) were cells transfected with both plasmids ligated with gRNA 1 and gRNA2 in a 1:1 proportion.

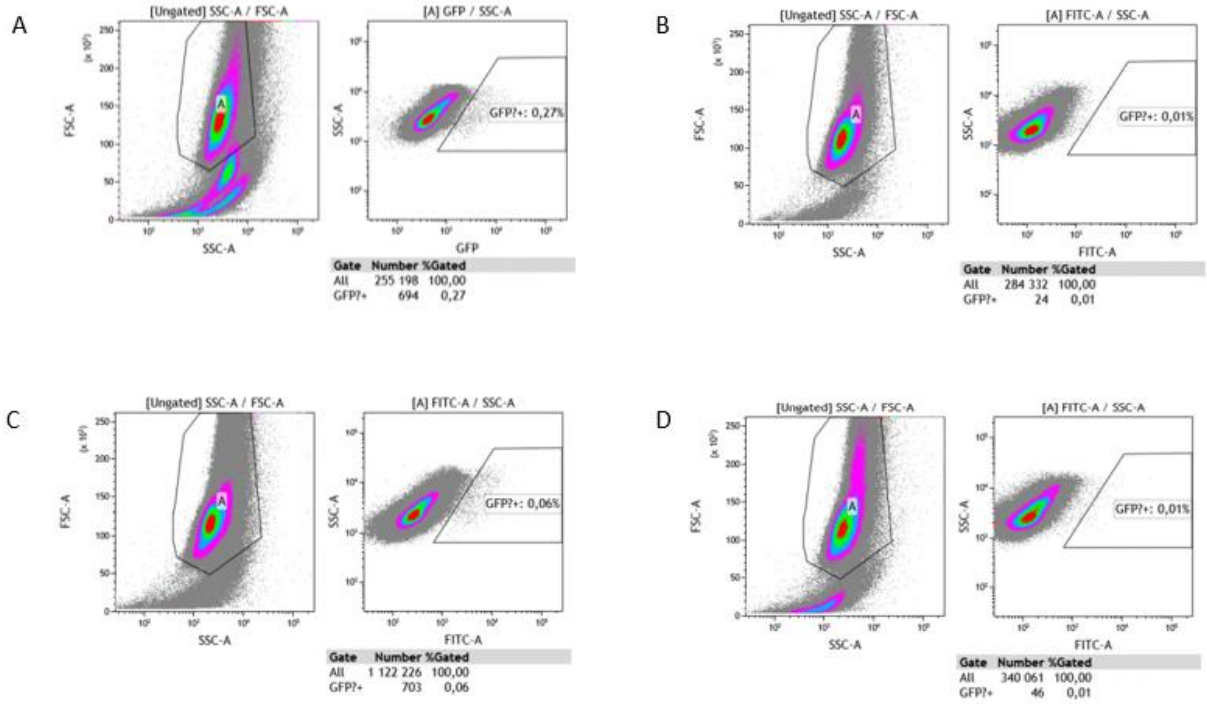

Figure 3.7. Illustration of the settings used on the FACS *(BD Facs Aria Fusion). A-D) shows both Forward (FSC-A) and side scatter (SSC-A) plot is used to separate cells according to size and granularity, respectively. The P1 gate is set as to exclude cellular debris (typically found in the lower-left handside corner) and clumps of cells, imperfectly isolated (typically found in the upper right onside corner). A denotes scatter plot of control untransfected cells whilst B,C and D are scatter plots of transfected cells with gRNA1, gRNA2 and combination of gRNA1 and gRNA2, respectively.*

3.6. Heteroduplex mobility assay (HMA)

In order to determine the presence of an NFκB knockout due to insertion or deletion, HMA was utilised. A PCR was run as previously described in Section 2.13. Genomic DNA from each cell pool was used. Figures 3.8 A), B) and C), shows genes from cells transfected with gRNA 1, gRNA 2 and both gRNA 1 and gRNA 2, respectively. 1, gRNA 2 and both gRNA 1 and gRNA 2, respectively and were mixed with control. Figure 3.8 shows bands at 578 bp only, meaning homogeneity or that there was no mutation-induced knockout in the cells.

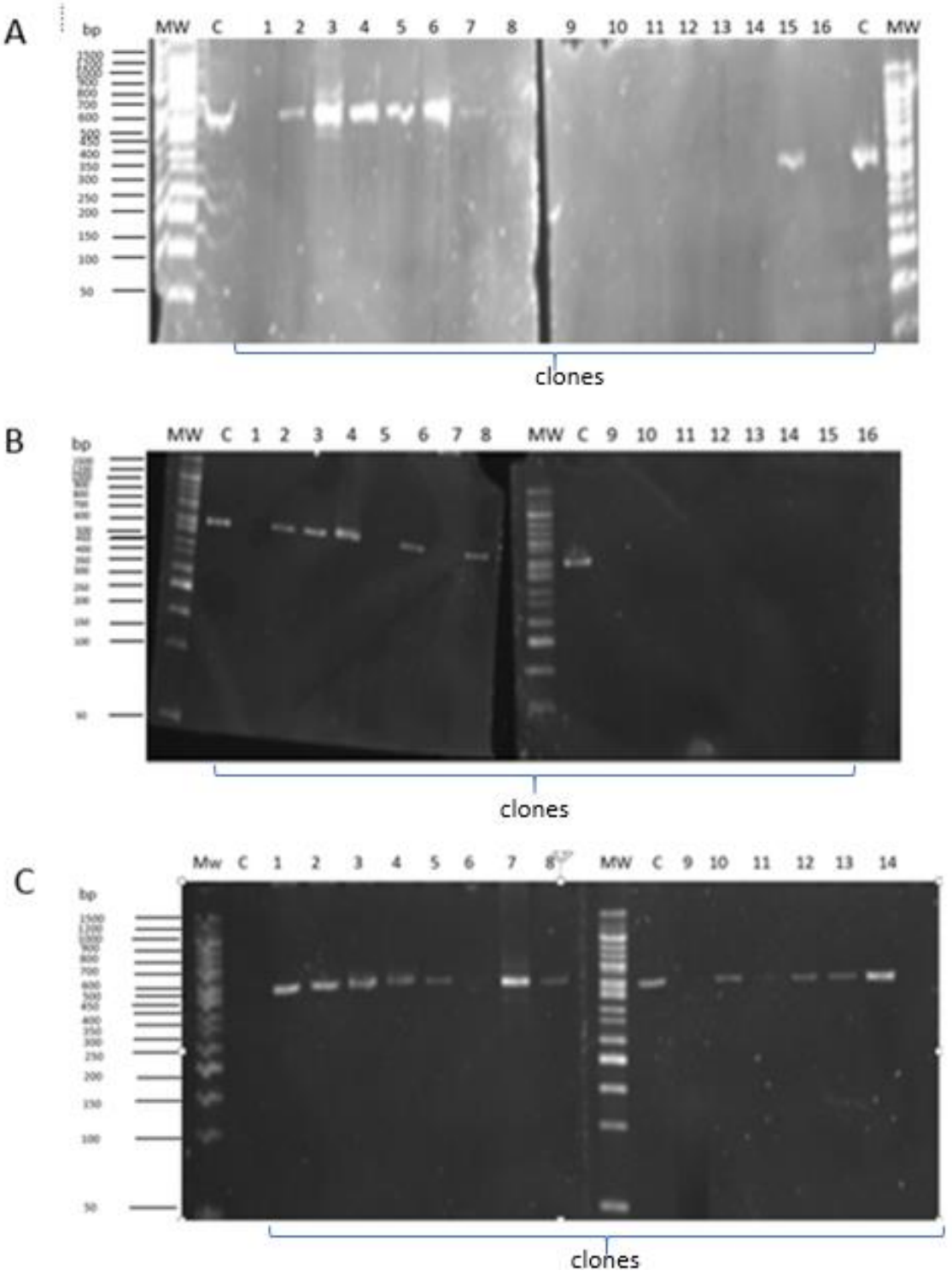

Figure 3.8. An illustration showing HMA results *with A) representing a group of cells transfected with gRNA 1, B) transfect with gRNA 2 and C transfected with both gRNA 1 and gRNA 2. The single band shows either non-knockout or homogenous knockout. MW is the molecular weight; C is the experimental control and 1 - 14 are samples. Amplicons were visualised after separation on 8 % TBE polyacrylamide gel stained in 0.5 µg/ml ethidium bromide.*

Figures 3.9 A), B) and C) shows genes from cells transfected with gRNA amplicons to check heterogeneity. Arrow in Figure 3.9 C shows a pair of extra bands as compared to the control lane. This indicates that when mixing amplicons with the controls, there was a mismatch due to heterogeneity.

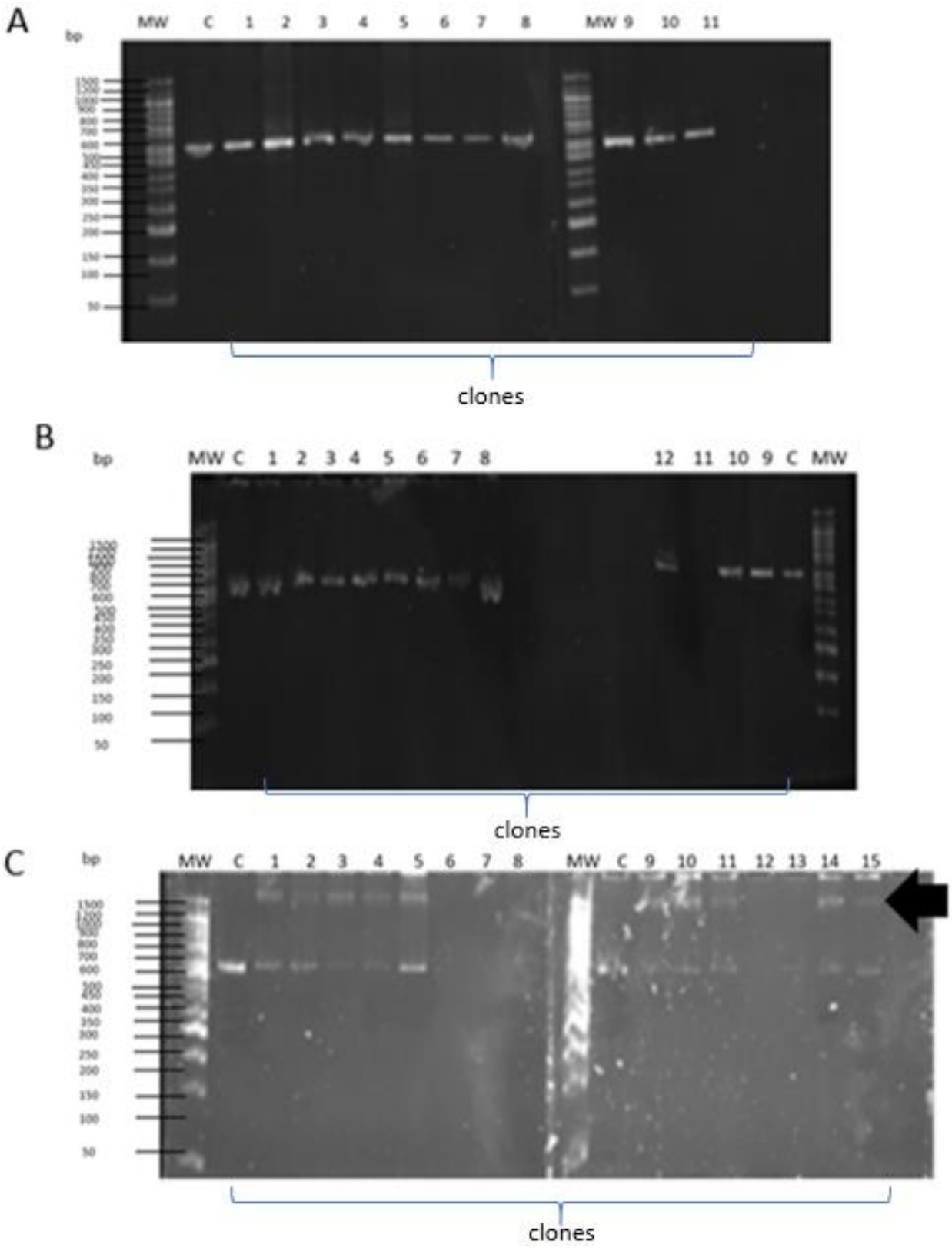

Figure 3.9. An illustration showing HMA results *with A) representing a group of cells treated with gRNA 1, B) treated with gRNA 2 and C treated by both gRNA 1 and gRNA 2. The single band confirms knockout. MW denotes molecular weight markers; C is the experimental control and 1-15 are the samples. Amplicons were visualised after separation on 8 % TBE polyacrylamide gel and then stained with 0.5 µg/ml ethidium bromide*

3.7. Western blot

The NFκB protein expression was confirmed by Western blotting. This was to validate if there was a knockdown in the *NFκB* gene. Figure 3.10 shows blot membranes treated with α- NFκB antibodies with lanes MW and C representing molecular marker and control, respectively. Lanes 1 through 15 represent samples from 3.9. C. Figure 3.10. B) shows membrane treated with α-actin antibodies as a loading control. Neither of the two membranes showed a band except for molecular marker. The expected band sizes were 105 or 50 kDa for NFκB1 proteins in Rel protein-specific transcription inhibitor and DNA binding subunit protein complex, respectively. As for actin, the expected band was 42 kDa. Wild type DNA was used as positive control. Western blots were repeated four times.

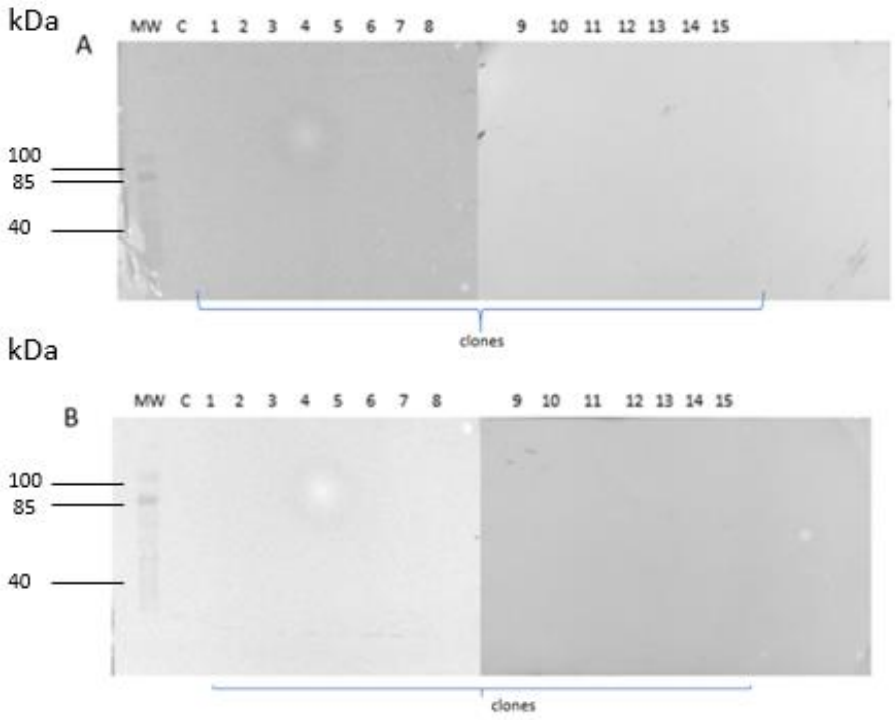

Figure 3.10. a membrane after *blotting. A) panel showing membrane targeting the NFκB 1 protein and B) showing the actin panel used as a loading control. In both blots, MW represents the molecular weight, C represents the experimental control, and 1-15 shows respective samples.*

Chapter 4: Discussion

HIV is one of the global disease burdens currently with just below 40 million people living with it worldwide, and 62 % of those are on treatment (UNAIDS, 2020). Whilst the disease is manageable; previous studies have shown the long-term side effects of ARV, which include insulin resistance. South Africa is amongst one of the countries with about 7.5 million of people living with the virus (UNAIDS, 2020). According to Statistics South Africa's 2019 report, diabetes is a leading non-communicable disease cause of death (STATS SA, 2020)..

In the current study, the aim was to understand the role NFκB pathway plays in insulin-resistance caused by ARVs. In order to achieve that, CRISPR cas9 was used to induce indels, which leads to gene knockout. One of the limiting issues of CRISPR is off-target effects. The gRNAs produced in this study had a minimum mismatch two and zero, respectively (Figure 3.1 and 3.2). This minimum mismatch shows that it is most unlikely to knock-out any other gene except the gene of interest, thus limiting the chance of off-target effects. This observation is in line with recommandations from Ran *et al.,* 2013 which include the analysis through an exhaustive search in the genome for off-target sequences that are similar to the guide sequence. Ideally, a good gRNA should fit the following; (i) be position-dependent: the 8–14 bp on the 3′ end of the guide sequence is less tolerant of mismatches than the 5′ bases, and (ii) be quantity dependent: in general, more than three mismatches are not tolerated; (iii) guide sequence-dependent: some guide sequences are less tolerant of mismatches than others. The CRISPR Design Tool integrates these criteria to provide predictions for likely off-target sites in the target genome.

After ligation and transformation, PCR was performed to confirm ligation. An expected amplicon of 333 and 333 bp for gRNA 1 and gRNA 2 respectively was determined with Snapgene program. Figure 3.4. shows ligated PCR products obtained by direct PCR amplification. PCR products match the expected size except for clone number 10 that showed a larger band size. This anomaly could be the results of an insertion mutation during cell growth. Mutations generally occur during replication, mitosis or other DNA damage. As noted in Figure 3.6, the sequence shows insertions of numerous nucleotides. Sequencing also played

a crucial role in confirming ligation. As seen in Figure 3.4, clone 4 and 23 on either plasmid showed a perfect match on gRNAs ligated (highlighted by blue). We have confidence in the sequencing results as the Phred score was found to be equal to 50. A Phred score of 50 translates that the probability of incorrect base call is 1 in 100,000 with a base call accuracy of 99.999 %.

These clones were then used for transfection. After transfection, FACS was performed to sort cells into a single cells per well. This was done to isolate a colony of the same clone. As a control, non-transfected cells were included. The total fluorescence recorded was 0.27 %. This is due to background noise generated either by auto-fluorescent or spectral overlap . A low fluorescence level compared to the control was recorded from all the experimental groups, with gRNA 1 and gRNA 1 and gRNA 2 both recording a 0.01 % and gRNA 2 group recording a 0.06 %. This could be due pSpCas9(BB)-2A-GFP (pX458) plasmid failure to express GFP, or insufficient plasmid was transfected due to competition amongst DNAs. However, we continued with the experiment because the main aim of performing FACS was to sort cell and grow a population of cells from single clones.

Several post-amplification methods can be used to rapidly analyse sequence variation in PCR products which includes restriction fragment length polymorphism (RFLP) (Ellis and Zambon, 2001). However, with RFLP polymorphisms in the nucleotides in the gene of interest may lead to loss of restriction sites. For this study, HMA was used because its easy to perform, quick and fairly inexpensive . HMA assesses the variation between amplicon of the potential knocked out gene and that of reference clone (Ellis and Zambon, 2001). The variation is shown by generating mismatches, that is heteroduplex after denaturation and renaturation (Ellis and Zambon, 2001).

Ideally, heteroduplexes migrate slower than the homoduplex of the same size due tothe divergence between two sequences in the mixture (Delward *et al*, 1995). At least 10 heteroduplexes, were produced in this study (Figure 3.9), inferring there was a mismatch in sequences. No clear heteroduplexes were observed on either Figure 3.13. A or B. This observation could mean that for a convincing knockout, more than one gRNAs need to be transfected concurrently. This method is in line with what Ellis and Zambon in 2001 observed in their influenza virus screening experiment. These results confirm that there was a NHEJ which caused a mutation on the gene of interest.

Western blot is a crucial technique in cell and molecular biology in assessing protein expression, among others. In this project, Western blot was used to determine if the was any knockdown in the experimental cell culture. The wild type cells were included for comparison. As it can be seen in Figure 3.10 A, no bands were visible for NFκB 1 protein nor on figure 3.15 B for actin protein which was included as a loading control. The objective was to determine if the NFκB protein was expressed to confirm the gene knockout. There may be several reasons for observing no bands. These reasons include but not limited to a low concentration of antigen or protein and non-fat milk masking the antigen (Mahmood and Yang, 2012). It may also be due contaminated buffer by contaminants like sodium azide, which in activates horse reddish peroxide activity (Mahmood and Yang, 2012). Improper antibodies or antibody concentration use and prolonged washing may also cause no signal in western blots (Mahmood and Yang, 2012).

In conclusion, the gene knock out was successful although the study could not elucidate the importance of Nfkb insulin resistance. The project built a strong foundation in understanding the processes of CRISPR. This can be used for future studies with ease. For future studies, gene expression levels confirmed by Western blotting could be developed and standardised to assess gene knockout.

References

ABOUD, M., ELGALIB, A., KULASEGARAM, R. & PETERS, B. 2007. Insulin resistance and HIV infection: a review. *International Journal of Clinical Practice,* 61**,** 463-472.

AGUIRRE, V., UCHIDA, T., YENUSH, L., DAVIS, R. & WHITE, M. F. 2000. The c-Jun NH2-terminal kinase promotes insulin resistance during association with insulin receptor substrate-1 and phosphorylation of Ser307. *Journal of Biological Chemistry,* 275**,** 9047-9054.

AGUIRRE, V., WERNER, E. D., GIRAUD, J., LEE, Y. H., SHOELSON, S. E. & WHITE, M. F. 2002. Phosphorylation of Ser307 in insulin receptor substrate-1 blocks interactions with the insulin receptor and inhibits insulin action. *Journal of Biological Chemistry,* 277**,** 1531-1537.

AHMED, Z. & PILLAY, T. S. 2003. Adapter protein with a pleckstrin homology (PH) and an Src homology 2 (SH2) domain (APS) and SH2-B enhance insulin-receptor autophosphorylation, extracellular-signal-regulated kinase and phosphoinositide 3-kinase-dependent signalling. *Biochemical Journal,* 371**,** 405-412.

AKASH, M. S. H., REHMAN, K. & CHEN, S. 2013. Role of inflammatory mechanisms in pathogenesis of type 2 diabetes mellitus. *Journal of Cellular Biochemistry,* 114**,** 525-531.

AKASH, M. S. H., REHMAN, K. & LIAQAT, A. 2018. Tumor Necrosis Factor-Alpha: Role in Development of Insulin Resistance and Pathogenesis of Type 2 Diabetes Mellitus. *Journal of Cellular Biochemistry,* 119**,** 105-110.

ALEXANDER, W. S. & HILTON, D. J. 2004. The role of suppressors of cytokine signaling (SOCS) proteins in regulation of the immune response. *Annual Review of Immunology,* 22**,** 503-529.

ANDERS, C., NIEWOEHNER, O., DUERST, A. & JINEK, M. 2014. Structural basis of PAM-dependent target DNA recognition by the Cas9 endonuclease. *Nature,* 513**,** 569.

APOSTOLOVA ,N; BLAS-GARCÍA, A & ESPLUGUES, J. 2011. Mitochondrial interference by anti-HIV drugs: mechanisms beyond Pol-γ inhibition. *Trends Pharmacological Science*, 32(12):715-25.

ARAGNO, M., MASTROCOLA, R., MEDANA, C., CATALANO, M. G., VERCELLINATTO, I., DANNI, O. & BOCCUZZI, G. 2006. Oxidative stress-dependent impairment of cardiac-specific transcription factors in experimental diabetes. *Endocrinology,* 147**,** 5967-5974.

ARTS, E. J. & HAZUDA, D. J. 2012. HIV-1 antiretroviral drug therapy. *Cold Spring Harbor Perspectives in Medicine***,** a007161.

ARKAN, M. C., HEVENER, A. L., GRETEN, F. R., MAEDA, S., LI, Z.-W., LONG, J. M., WYNSHAW-BORIS, A., POLI, G., OLEFSKY, J. & KARIN, M. 2005. IKK-β links inflammation to obesity-induced insulin resistance. *Nature Medicine,* 11**,** 191.

ATKINSON, B. J., GRIESEL, B. A., KING, C. D., JOSEY, M. A. & OLSON, A. L. 2013. Moderate GLUT4 overexpression improves insulin sensitivity and fasting triglyceridemia in high fat fed transgenic mice. *Diabetes***,** DB_121146.

AVERT 2019, viewed 04 April 2020 <https://www.avert.org/professionals/hiv-around-world/sub-saharan-africa/south-africa,

BEN-ROMANO, R., RUDICH, A., ETZION, S., POTASHNIK, R., KAGAN, E., GREENBAUM, U. & BASHAN, N. 2006. Nelfinavir induces adipocyte insulin resistance through the

induction of oxidative stress: differential protective effect of antioxidant agents. *Antiviral Therapy,* 11**,** 1051.

BJØRBÆK, C., ELMQUIST, J. K., FRANTZ, J. D., SHOELSON, S. E. & FLIER, J. S. 1998. Identification of SOCS-3 as a potential mediator of central leptin resistance. *Molecular Cell,* 1**,** 619-625.

BOGDANOVE, A. J., SCHORNACK, S. & LAHAYE, T. 2010. TAL effectors: finding plant genes for disease and defense. *Current Opinion in Plant Biology,* 13**,** 394-401.

BOHUSLAV, J., KRAVCHENKO, V. V., PARRY, G. C., ERLICH, J. H., GERONDAKIS, S., MACKMAN, N. & ULEVITCH, R. J. 1998. Regulation of an essential innate immune response by the p50 subunit of NF-kappaB. *The Journal of Clinical Investigation,* 102**,** 1645-1652.

CAI, D., YUAN, M., FRANTZ, D. F., MELENDEZ, P. A., HANSEN, L., LEE, J. & SHOELSON, S. E. 2005. Local and systemic insulin resistance resulting from hepatic activation of IKK-β and NFκB. *Nature Medicine,* 11**,** 183

CARPER, M. J., CADE, W. T., CAM, M., ZHANG, S., SHALEV, A., YARASHESKI, K. E. & RAMANADHAM, S. 2008. HIV-protease inhibitors induce expression of suppressor of cytokine signaling-1 in insulin-sensitive tissues and promote insulin resistance and type 2 diabetes mellitus. *American Journal of Physiology. Endocrinology and Metabolism,* 294**,** E558.

CARTER-KENT, C., ZEIN, N. N. & FELDSTEIN, A. E. 2008. Cytokines in the pathogenesis of fatty liver and disease progression to steatohepatitis: implications for treatment. *The American Journal of Gastroenterology,* 103**,** 1036.

CHA, D. R., KANG, Y. S., HAN, S. Y., JEE, Y. H., HAN, K. H., KIM, H. K., HAN, J. Y. & KIM, Y. S. 2005. Role of aldosterone in diabetic nephropathy. *Nephrology,* 10**,** S37-S39.

CHAN, S. M., SUN, R.-Q., ZENG, X.-Y., CHOONG, Z.-H., WANG, H., WATT, M. J. & YE, J.-M. 2013. Activation of PPARα ameliorates hepatic insulin resistance and steatosis in high fructose-fed mice despite increased ER stress. *Diabetes***,** DB_121397.

CHAPARRO, J., REEDS, D. N., WEN, W., XUEPING, E., KLEIN, S., SEMENKOVICH, C. F., BAE, K. T., QUIRK, E. K., POWDERLY, W. G. & YARASHESKI, K. E. 2005. Alterations in thigh subcutaneous adipose tissue gene expression in protease inhibitor-based highly active antiretroviral therapy. *Metabolism,* 54**,** 561-567.

CHO, S. W., KIM, S., KIM, J. M. & KIM, J.-S. 2013. Targeted genome engineering in human cells with the Cas9 RNA-guided endonuclease. *Nature Biotechnology,* 31**,** 230.

CHRISTIAN, M., CERMAK, T., DOYLE, E. L., SCHMIDT, C., ZHANG, F., HUMMEL, A., BOGDANOVE, A. J. & VOYTAS, D. F. 2010. Targeting DNA double-strand breaks with TAL effector nucleases. *Genetics,* 186**,** 757-761.

COHEN, C. D., FRACH, K., SCHLÖNDORFF, D. & KRETZLER, M. 2002. Quantitative gene expression analysis in renal biopsies: a novel protocol for a high-throughput multicenter application. *Kidney International,* 61**,** 133-140.

CONG, L., RAN, F. A., COX, D., LIN, S., BARRETTO, R., HABIB, N., HSU, P. D., WU, X., JIANG, W. & MARRAFFINI, L. 2013. Multiplex genome engineering using CRISPR/Cas systems. *Science***,** 1231143.

DA ROCHA, A. F., LIBONI, T. F., KURAUTI, M. A., DE SOUZA, C. O., MIKSZA, D. R., MOREIRA, C. C. L., BORBA-MURAD, G. R., BAZOTTE, R. B. & DE SOUZA, H. M. 2014. Tumor necrosis factor alpha abolished the suppressive effect of insulin on hepatic glucose production and glycogenolysis stimulated by cAMP. *Pharmacological Reports,* 66**,** 380-385.

DEAN, M., CARRINGTON, M., WINKLER, C., HUTTLEY, G. A., SMITH, M. W., ALLIKMETS, R., GOEDERT, J. J., BUCHBINDER, S. P., VITTINGHOFF, E. & GOMPERTS, E. 1996. Genetic restriction of HIV-1 infection and progression to AIDS by a deletion allele of the CKR5 structural gene. *Science,* 273**,** 1856-1862.

DELTCHEVA, E., CHYLINSKI, K., SHARMA, C. M., GONZALES, K., CHAO, Y., PIRZADA, Z. A., ECKERT, M. R., VOGEL, J. & CHARPENTIER, E. 2011. CRISPR RNA maturation by trans-encoded small RNA and host factor RNase III. *Nature,* 471**,** 602.

DJEDAINI, M., PERALDI, P., DRICI, M.-D., DARINI, C., SAINT-MARC, P., DANI, C. & LADOUX, A. 2009. Lopinavir co-induces insulin resistance and ER stress in human adipocytes. *Biochemical and Biophysical Research Communications,* 386**,** 96-100.

DONG, Y., DEKENS, D. W., DE DEYN, P. P., NAUDÉ, P. J. & EISEL, U. L. 2015. Targeting of tumor necrosis factor alpha receptors as a therapeutic strategy for neurodegenerative disorders. *Antibodies,* 4**,** 369-408.

DUAN, C., YANG, H., WHITE, M. F. & RUI, L. 2004. Disruption of the SH2-B gene causes age-dependent insulin resistance and glucose intolerance. *Molecular and Cellular Biology,* 24**,** 7435-7443.

DUNN, S. L., BJÖRNHOLM, M., BATES, S. H., CHEN, Z., SEIFERT, M. & MYERS JR, M. G. 2005. Feedback inhibition of leptin receptor/Jak2 signaling via Tyr1138 of the leptin receptor and suppressor of cytokine signaling 3. *Molecular Endocrinology,* 19**,** 925-938.

EBERLE, J; GURTLER, L. 2012. HIV Types, Groups, Subtypes and Recombinant Forms: Errors in Replication, Selection Pressure and Quasispecies. *Intervirology*, 55:79–83

EHLERS, S. 2003. Role of tumour necrosis factor (TNF) in host defence against tuberculosis: implications for immunotherapies targeting TNF. *Annals of the Rheumatic Diseases,* 62**,** ii37-ii42.

EMANUELLI, B., PERALDI, P., FILLOUX, C., SAWKA-VERHELLE, D., HILTON, D. & VAN OBBERGHEN, E. 2000. SOCS-3 is an insulin-induced negative regulator of insulin signaling. *Journal of Biological Chemistry,* 275**,** 15985-15991.

ESPOSITO, K., NAPPO, F., MARFELLA, R., GIUGLIANO, G., GIUGLIANO, F., CIOTOLA, M., QUAGLIARO, L., CERIELLO, A. & GIUGLIANO, D. 2002. Inflammatory cytokine concentrations are acutely increased by hyperglycemia in humans: role of oxidative stress. *Circulation,* 106**,** 2067-2072.

ESTEBAN, V., RUPEREZ, M., VITA, J. R., LÓPEZ, E. S., MEZZANO, S., PLAZA, J. J., EGIDO, J. & RUIZ-ORTEGA, M. 2003. Effect of simultaneous blockade of AT1 and AT2 receptors on the NFκB pathway and renal inflammatory response. *Kidney International,* 64**,** S33-S38.

FASSHAUER, M. & PASCHKE, R. 2003. Regulation of adipocytokines and insulin resistance. *Diabetologia,* 46**,** 1594-1603.

FISCHER, R. & MAIER, O. 2015. Interrelation of oxidative stress and inflammation in neurodegenerative disease: role of TNF. *Oxidative medicine and cellular longevity,* 2015.

FISHER, J. S., GAO, J., HAN, D.-H., HOLLOSZY, J. O. & NOLTE, L. A. 2002. Activation of AMP kinase enhances sensitivity of muscle glucose transport to insulin. *American Journal of Physiology-Endocrinology And Metabolism,* 282**,** E18-E23.

GAJ, T., SIRK, S. J., SHUI, S.-L. & LIU, J. 2016. Genome-editing technologies: principles and applications. *Cold Spring Harbor Perspectives in Biology***,** a023754.

GAO, F., BAILES, E., ROBERTSON, D. L., CHEN, Y., RODENBURG, C. M., MICHAEL, S. F., CUMMINS, L. B., ARTHUR, L. O., PEETERS, M. & SHAW, G. M. 1999. Origin of HIV-1 in the chimpanzee Pan troglodytes troglodytes. *Nature,* 397**,** 436.

GAO, Z., HE, Q., PENG, B., CHIAO, P. J. & YE, J. 2006. Regulation of nuclear translocation of HDAC3 by IκBα is required for tumor necrosis factor inhibition of peroxisome proliferator-activated receptor γ function. *Journal of Biological Chemistry,* 281**,** 4540-4547.

GARVEY, W., MAIANU, L., HUECKSTEADT, T., BIRNBAUM, M., MOLINA, J. & CIARALDI, T. 1991. Pretranslational suppression of a glucose transporter protein causes insulin resistance in adipocytes from patients with non-insulin-dependent diabetes mellitus and obesity. *The Journal of Clinical Investigation,* 87**,** 1072-1081.

GELDERBLOM, H. R. 1991. Assembly and morphology of HIV: potential effect of structure on viral function. *Aids,* 5**,** 617-638.

GRISSA, I., VERGNAUD, G. & POURCEL, C. 2007. CRISPRFinder: a web tool to identify clustered regularly interspaced short palindromic repeats. *Nucleic Acids Research,* 35**,** W52-W57.

GROBLER, J. A., STILLMOCK, K., HU, B., WITMER, M., FELOCK, P., ESPESETH, A. S., WOLFE, A., EGBERTSON, M., BOURGEOIS, M. & MELAMED, J. 2002. Diketo acid inhibitor mechanism and HIV-1 integrase: implications for metal binding in the active site of phosphotransferase enzymes. *Proceedings of the National Academy of Sciences,* 99**,** 6661-6666.

HAAK, E. S., USADEL, K. H., KOHLEISEN, M., YILMAZ, A., KUSTERER, K. & HAAK, T. 1999. The effect of α-lipoic acid on the neurovascular reflex arc in patients with diabetic neuropathy assessed by capillary microscopy. *Microvascular Research,* 58**,** 28-34.

HARADA, C., OKUMURA, A., NAMEKATA, K., NAKAMURA, K., MITAMURA, Y., OHGURO, H. & HARADA, T. 2006. Role of monocyte chemotactic protein-1 and nuclear factor kappa B in the pathogenesis of proliferative diabetic retinopathy. *Diabetes Research and Clinical Practice,* 74**,** 249-256.

HAYDEN, M. S. & GHOSH, S. 2008. Shared principles in NFκB signaling. *Cell,* 132**,** 344-362.

HAYDEN, M. S. & GHOSH, S. 2012. NFκB, the first quarter-century: remarkable progress and outstanding questions. *Genes and Development,* 26**,** 203-234.

HILTON, D. J., RICHARDSON, R. T., ALEXANDER, W. S., VINEY, E. M., WILLSON, T. A., SPRIGG, N. S., STARR, R., NICHOLSON, S. E., METCALF, D. & NICOLA, N. A. 1998. Twenty proteins containing a C-terminal SOCS box form five structural classes. *Proceedings of the National Academy of Sciences,* 95**,** 114-119.

HIROSUMI, J., TUNCMAN, G., CHANG, L., GÖRGÜN, C. Z., UYSAL, K. T., MAEDA, K., KARIN, M. & HOTAMISLIGIL, G. S. 2002. A central role for JNK in obesity and insulin resistance. *Nature,* 420**,** 333.

HOESEL, B. & SCHMID, J. A. 2013. The complexity of NFκB signaling in inflammation and cancer. *Molecular Cancer,* 12**,** 86.

HORVATH, P. & BARRANGOU, R. 2010. CRISPR/Cas, the immune system of bacteria and archaea. *Science,* 327**,** 167-170.

HOTAMISLIGIL, G. S., ARNER, P., CARO, J. F., ATKINSON, R. L. & SPIEGELMAN, B. M. 1995. Increased adipose tissue expression of tumor necrosis factor-alpha in human obesity and insulin resistance. *The Journal of Clinical Investigation,* 95**,** 2409-2415.

HOTAMISLIGIL, G. S., MURRAY, D. L., CHOY, L. N. & SPIEGELMAN, B. M. 1994. Tumor necrosis factor alpha inhibits signaling from the insulin receptor. *Proceedings of the National Academy of Sciences,* 91**,** 4854-4858.

HOTAMISLIGIL, G. S., SHARGILL, N. S. & SPIEGELMAN, B. M. 1993. Adipose expression of tumor necrosis factor-alpha: direct role in obesity-linked insulin resistance. *Science,* 259**,** 87-91.

HOWARD, J. K. & FLIER, J. S. 2006. Attenuation of leptin and insulin signaling by SOCS proteins. *Trends in Endocrinology & Metabolism,* 17**,** 365-371.

HSU, P. D., LANDER, E. S. & ZHANG, F. 2014. Development and applications of CRISPR-Cas9 for genome engineering. *Cell,* 157**,** 1262-1278.

HUANG, S. & CZECH, M. P. 2007. The GLUT4 glucose transporter. *Cell Metabolism,* 5**,** 237-252.

HUANG, X; GONG, R; LI, X; VIRTUE, A; YANG, F; YANG, I; TRAN, A; YANG, X & WANG, H. 2013. Identification of novel pretranslational regulatory mechanisms for NFκB activation. *The Journal Of Biological Chemistry*, 288, 15628 –15640.

IKEMOTO, S., THOMPSON, K. S., ITAKURA, H., LANE, M. D. & EZAKI, O. 1995. Expression of an insulin-responsive glucose transporter (GLUT4) minigene in transgenic mice: effect of exercise and role in glucose homeostasis. *Proceedings of the National Academy of Sciences,* 92**,** 865-869.

ISMAIL, W., KING, J. & PILLAY, T. S. 2009. Insulin resistance induced by antiretroviral drugs: Current understanding of molecular mechanisms. *Journal of Endocrinology, Metabolism and Diabetes of South Africa,* 14**,** 129-132.

ISMAIL, W.I.W., KING, J.A., ANWAR, K. & PILLAY, T.S. 2013. Indinavir and nelfinavir inhibit proximal insulin receptor signaling and salicylate abrogates inhibition: potential role of the NFkappa B pathway. *Journal of Clinical Biochemistry,*114, 1729-1737.

JABALAMELI, H. R., ZAHEDNASAB, H., KARIMI-MOGHADDAM, A. & JABALAMELI, M. R. 2015. Zinc finger nuclease technology: advances and obstacles in modelling and treating genetic disorders. *Gene,* 558**,** 1-5.

JIANG, F. & DOUDNA, J. F. 2017. CRISPR-Cas9 structures and mechanisms. *Annual Reviews,* 46:1 505-529

JORGENSEN, S. B., O'NEILL, H. M., SYLOW, L., HONEYMAN, J., HEWITT, K. A., PALANIVEL, R., FULLERTON, M. D., ÖBERG, L., BALENDRAN, A. & GALIC, S. 2012. Deletion of skeletal muscle SOCS3 prevents insulin resistance in obesity. *Diabetes***,** DB_120443.

KERN, P. A., RANGANATHAN, S., LI, C., WOOD, L. & RANGANATHAN, G. 2001. Adipose tissue tumor necrosis factor and interleukin-6 expression in human obesity and insulin resistance. *American Journal of Physiology-Endocrinology And Metabolism,* 280**,** E745-E751.

KIM, D., BAE, S., PARK, J., KIM, E., KIM, S., YU, H. R., HWANG, J., KIM, J.-I. & KIM, J.-S. 2015. Digenome-seq: genome-wide profiling of CRISPR-Cas9 off-target effects in human cells. *Nature Methods,* 12**,** 237.

KLUG, A. 2010. The discovery of zinc fingers and their applications in gene regulation and genome manipulation. *Annual Review of Biochemistry,* 79**,** 213-231.

KOHLSTAEDT, L., WANG, J., FRIEDMAN, J., RICE, P. & STEITZ, T. 1992. Crystal structure at 3.5 A resolution of HIV-1 reverse transcriptase complexed with an inhibitor. *Science,* 256**,** 1783-1790.

KUSCU, C., ARSLAN, S., SINGH, R., THORPE, J. & ADLI, M. 2014. Genome-wide analysis reveals characteristics of off-target sites bound by the Cas9 endonuclease. *Nature Biotechnology,* 32**,** 677.

LAGATHU, C., EUSTACE, B., PROT, M., FRANTZ, D., GU, Y., BASTARD, J.-P., MAACHI, M., AZOULAY, S., BRIGGS, M. & CARON, M. 2007. Some HIV antiretrovirals increase oxidative stress and alter chemokine, cytokine or adiponectin production in human adipocytes and macrophages. *Antiviral Therapy,* 12**,** 489.

LEBRUN, P. & VAN OBBERGHEN, E. 2008. SOCS proteins causing trouble in insulin action. *Acta Physiologica,* 192**,** 29-36.

LETO, D. & SALTIEL, A. R. 2012. Regulation of glucose transport by insulin: traffic control of GLUT4. *Nature reviews Molecular Cell Biology,* 13**,** 383.

LUWIC, P,A. Human Imuunonodeficiency virus and their replication. In: Fields, B. N., Knipe. D., M., Howley, P.M., Chanock, R. M, Melnic, J. L., Monath, T. P., Roizman, B. & Srwaus, S. E. Editors, Field virology, 3rd ed. Philadelphia Pa: Lippincott-Raven Publishers, 1996 pp 1881-1952

MALI, P., YANG, L., ESVELT, K. M., AACH, J., GUELL, M., DICARLO, J. E., NORVILLE, J. E. & CHURCH, G. M. 2013. RNA-guided human genome engineering via Cas9. *Science,* 339**,** 823-826.

MATTHEWS, T; SALGO, M; GREENBERG, M; CHUNG, J; DEMASI, R & BOLOGNESI, D. (2004). Enfuvirtide: the first therapy to inhibit the entry of HIV-1 into host CD4 lymphocytes. *Nature review:drug descover,* **3**, 215–225.

MATTSON, M. P. & CAMANDOLA, S. 2001. NFκB in neuronal plasticity and neurodegenerative disorders. *The Journal of Clinical Investigation,* 107**,** 247-254.

MAURES, T. J., CHEN, L. & CARTER-SU, C. 2009. Nucleocytoplasmic shuttling of the adapter protein SH2B1β (SH2-Bβ) is required for nerve growth factor (NGF)-dependent neurite outgrowth and enhancement of expression of a subset of NGF-responsive genes. *Molecular Endocrinology,* 23**,** 1077-1091.

MAY, M. J. & GHOSH, S. Rel/NFκB and IκB proteins: an overview. Seminars in cancer biology, 1997. Elsevier, 63-73.

MERCER, T. R., GERHARDT, D. J., DINGER, M. E., CRAWFORD, J., TRAPNELL, C., JEDDELOH, J. A., MATTICK, J. S. & RINN, J. L. 2012. Targeted RNA sequencing reveals the deep complexity of the human transcriptome. *Nature Biotechnology,* 30**,** 99.

MILLER, J. C., TAN, S., QIAO, G., BARLOW, K. A., WANG, J., XIA, D. F., MENG, X., PASCHON, D. E., LEUNG, E. & HINKLEY, S. J. 2011. A TALE nuclease architecture for efficient genome editing. *Nature Biotechnology,* 29**,** 143.

MOHAMED, A. K., BIERHAUS, A., SCHIEKOFER, S., TRITSCHLER, H., ZIEGLER, R. & NAWROTH, P. P. 1999. The role of oxidative stress and NF-κB activation in late diabetic complications. *Biofactors,* 10**,** 157-167.

MONIER, P. L. & WILCOX, R. 2004. Metabolic complications associated with the use of highly active antiretroviral therapy in HIV-1–infected adults. *The American Journal of the Medical Sciences,* 328**,** 48-56.

MORRIS, D. L., CHO, K. W., ZHOU, Y. & RUI, L. 2009. SH2B1 enhances insulin sensitivity by both stimulating the insulin receptor and inhibiting tyrosine dephosphorylation of IRS proteins. *Diabetes*.

MUECKLER, M. 2001. Insulin resistance and the disruption of Glut4 trafficking in skeletal muscle. *The Journal of Clinical Investigation,* 107**,** 1211-1213.

MURATA, H., HRUZ, P. W. & MUECKLER, M. 2000. The mechanism of insulin resistance caused by HIV protease inhibitor therapy. *Journal of Biological Chemistry,* 275**,** 20251-20254.

MURATA, H., HRUZ, P. W. & MUECKLER, M. 2002. Indinavir inhibits the glucose transporter isoform Glut4 at physiologic concentrations. *Aids,* 16**,** 859-863.

MUSHNI, A. 2012, DNA sequencing methods and application. InTech pubisher

NEUMAN,M; MONTEIRO, M; & REHM, J. 2009. Drug interactions betweenpsychoactive substances and antiretroviral therapy in individuals infected with human immunodeficiency and hepatitis viruses. *Substance Use & Misuse,* 41(10-12):1395-463

NOOR, M. A. 2007. The role of protease inhibitors in the pathogenesis of HIV-associated insulin resistance: cellular mechanisms and clinical implications. *Current HIV/AIDS Reports,* 4**,** 126-134.

PAZ, K., LIU, Y.-F., SHORER, H., HEMI, R., LEROITH, D., QUAN, M., KANETY, H., SEGER, R. & ZICK, Y. 1999. Phosphorylation of insulin receptor substrate-1 (IRS-1) by protein kinase B positively regulates IRS-1 function. *Journal of Biological Chemistry,* 274**,** 28816-28822.

PENDERGRASS, M., BERTOLDO, A., BONADONNA, R., NUCCI, G., MANDARINO, L., COBELLI, C. & DEFRONZO, R. A. 2007. Muscle glucose transport and phosphorylation in type 2 diabetic, obese nondiabetic, and genetically predisposed individuals. *American Journal of Physiology-Endocrinology and Metabolism,* 292**,** E92-E100.

PERKINS, N. & GILMORE, T. 2006. Good cop, bad cop: the different faces of NFκB. *Cell death and differentiation,* 13**,** 759.

QU, X., SEALE, J. & DONNELLY, R. 1999. Tissue and isoform-selective activation of protein kinase C in insulin-resistant obese Zucker rats-effects of feeding. *Journal of Endocrinology,* 162**,** 207-214.

RAN, F. A., HSU, P. D., LIN, C.-Y., GOOTENBERG, J. S., KONERMANN, S., TREVINO, A. E., SCOTT, D. A., INOUE, A., MATOBA, S. & ZHANG, Y. 2013a. Double nicking by RNA-guided CRISPR Cas9 for enhanced genome editing specificity. *Cell,* 154**,** 1380-1389.

RAN, F. A., HSU, P. D., WRIGHT, J., AGARWALA, V., SCOTT, D. A. & ZHANG, F. 2013b. Genome engineering using the CRISPR-Cas9 system. *Nature Protocols,* 8**,** 2281.

REN, D., LI, M., DUAN, C. & RUI, L. 2005. Identification of SH2-B as a key regulator of leptin sensitivity, energy balance, and body weight in mice. *Cell Metabolism,* 2**,** 95-104.

REN, D., ZHOU, Y., MORRIS, D., LI, M., LI, Z. & RUI, L. 2007. Neuronal SH2B1 is essential for controlling energy and glucose homeostasis. *The Journal of Clinical Investigation,* 117**,** 397-406.

RHODES, D. & KLUG, A. 1993. Zinc fingers. *Scientific American,* 268**,** 56-65.

RIEDEL, H., WANG, J., HANSEN, H. & YOUSAF, N. 1997. PSM, an insulin-dependent, pro-rich, PH, SH2 domain containing partner of the insulin receptor. *The Journal of Biochemistry,* 122**,** 1105-1113.

RUAN, H., HACOHEN, N., GOLUB, T. R., VAN PARIJS, L. & LODISH, H. F. 2002. Tumor necrosis factor-α suppresses adipocyte-specific genes and activates expression of preadipocyte genes in 3T3-L1 adipocytes: nuclear factor-κB activation by TNF-α is obligatory. *Diabetes,* 51**,** 1319-1336.

RUAN, H. & LODISH, H. F. 2003. Insulin resistance in adipose tissue: direct and indirect effects of tumor necrosis factor-α. *Cytokine & Growth Factor Reviews,* 14**,** 447-455.

RUAN, H., POWNALL, H. J. & LODISH, H. F. 2003. Troglitazone antagonizes tumor necrosis factor-α-induced reprogramming of adipocyte gene expression by inhibiting the transcriptional regulatory functions of NFκB. *Journal of Biological Chemistry,* 278**,** 28181-28192.

RUDICH, A., KONRAD, D., TÖRÖK, D., BEN-ROMANO, R., HUANG, C., NIU, W., GARG, R., WIJESEKARA, N., GERMINARIO, R. & BILAN, P. 2003. Indinavir uncovers different

contributions of GLUT4 and GLUT1 towards glucose uptake in muscle and fat cells and tissues. *Diabetologia,* 46**,** 649-658.

RUDICH, A., VANOUNOU, S., RIESENBERG, K., PORAT, M., TIROSH, A., HARMAN-BOEHM, I., GREENBERG, A. S., SCHLAEFFER, F. & BASHAN, N. 2001. The HIV protease inhibitor nelfinavir induces insulin resistance and increases basal lipolysis in 3T3-L1 adipocytes. *Diabetes,* 50**,** 1425-1431.

RUI, L. 2014. SH2B1 regulation of energy balance, body weight, and glucose metabolism. *World Journal of Diabetes,* 5**,** 511.

RUIZ-ORTEGA, M., LORENZO, O., RUPÉREZ, M., BLANCO, J. & EGIDO, J. 2001. Systemic infusion of angiotensin II into normal rats activates nuclear factor-κB and AP-1 in the kidney: role of AT1 and AT2 receptors. *The American Journal of Pathology,* 158**,** 1743-1756.

SABIO, G., KENNEDY, N. J., CAVANAGH-KYROS, J., JUNG, D. Y., KO, H. J., ONG, H., BARRETT, T., KIM, J. K. & DAVIS, R. J. 2010. Role of muscle c-Jun NH2-terminal kinase 1 in obesity-induced insulin resistance. *Molecular and Cellular Biology,* 30**,** 106-115.

SAKAI, N., WADA, T., FURUICHI, K., IWATA, Y., YOSHIMOTO, K., KITAGAWA, K., KOKUBO, S., KOBAYASHI, M., HARA, A. & YAMAHANA, J. 2005. Involvement of extracellular signal-regulated kinase and p38 in human diabetic nephropathy. *American Journal of Kidney Diseases,* 45**,** 54-65.

SCHÜTT, M., MEIER, M., MEYER, M., KLEIN, J., ARIES, S. & KLEIN, H. 2000. The HIV-1 protease inhibitor indinavir impairs insulin signalling in HepG2 hepatoma cells. *Diabetologia,* 43**,** 1145-1148.

SENN, J. J., KLOVER, P. J., NOWAK, I. A., ZIMMER, T. A., KONIARIS, L. G., FURLANETTO, R. W. & MOONEY, R. A. 2003. Suppressor of cytokine signaling-3 (SOCS-3): A potential mediator of interleukin-6 dependent insulin resistance in hepatocytes. *Journal of Biological Chemistry*.

SHOELSON, S. E., LEE, J. & GOLDFINE, A. B. 2006. Inflammation and insulin resistance. *The Journal of Clinical Investigation,* 116**,** 1793-1801.

SHUKLA, V. K., DOYON, Y., MILLER, J. C., DEKELVER, R. C., MOEHLE, E. A., WORDEN, S. E., MITCHELL, J. C., ARNOLD, N. L., GOPALAN, S. & MENG, X. 2009. Precise genome modification in the crop species Zea mays using zinc-finger nucleases. *Nature,* 459**,** 437.

SOLINAS, G. & BECATTINI, B. 2017. JNK at the crossroad of obesity, insulin resistance, and cell stress response. *Molecular Metabolism,* 6**,** 174-184.

STATISTICS SOUTH AFRICA, ND.

STEIN, B. S., GOWDA, S. D., LIFSON, J. D., PENHALLOW, R. C., BENSCH, K. G. & ENGLEMAN, E. G. 1987. pH-independent HIV entry into CD4-positive T cells via virus envelope fusion to the plasma membrane. *Cell,* 49**,** 659-668.

SUZAWA, M., TAKADA, I., YANAGISAWA, J., OHTAKE, F., OGAWA, S., YAMAUCHI, T., KADOWAKI, T., TAKEUCHI, Y., SHIBUYA, H. & GOTOH, Y. 2003. Cytokines suppress adipogenesis and PPAR-γ function through the TAK1/TAB1/NIK cascade. *Nature Cell Biology,* 5**,** 224.

TAN, G; NIU,J; SHI, Y; OUYANG, H & WU, Z. 2012. NFκB-dependent microrna-125b up-regulation promotes. *The Journal Of Biological Chemistry*, 39, 33036 –33047
Cell Survival by Targeting p38 upon Ultraviolet Radiation

TANG, T., ZHANG, J., YIN, J., STASZKIEWICZ, J., GAWRONSKA-KOZAK, B., JUNG, D. Y., KO, H. J., ONG, H., KIM, J. K. & MYNATT, R. 2010. Uncoupling of inflammation and insulin

resistance by NFκB in transgenic mice through elevated energy expenditure. *Journal of Biological Chemistry,* 285**,** 4637-4644.

TANTI, J.-F., GREMEAUX, T., VAN OBBERGHEN, E. & LE MARCHAND-BRUSTEL, Y. 1994. Serine/threonine phosphorylation of insulin receptor substrate 1 modulates insulin receptor signaling. *Journal of Biological Chemistry,* 269**,** 6051-6057.

TORISU, T., SATO, N., YOSHIGA, D., KOBAYASHI, T., YOSHIOKA, T., MORI, H., IIDA, M. & YOSHIMURA, A. 2007. The dual function of hepatic SOCS3 in insulin resistance in vivo. *Genes to Cells,* 12**,** 143-154.

TSAO, T.-S., BURCELIN, R., KATZ, E. B., HUANG, L. & CHARRON, M. J. 1996. Enhanced insulin action due to targeted GLUT4 overexpression exclusively in muscle. *Diabetes,* 45**,** 28-36.

TUNCMAN, G., HIROSUMI, J., SOLINAS, G., CHANG, L., KARIN, M. & HOTAMISLIGIL, G. S. 2006. Functional in vivo interactions between JNK1 and JNK2 isoforms in obesity and insulin resistance. *Proceedings of the National Academy of Sciences,* 103**,** 10741-10746.

UEKI, K., KONDO, T. & KAHN, C. R. 2004a. Suppressor of cytokine signaling 1 (SOCS-1) and SOCS-3 cause insulin resistance through inhibition of tyrosine phosphorylation of insulin receptor substrate proteins by discrete mechanisms. *Molecular and Cellular Biology,* 24**,** 5434-5446.

UEKI, K., KONDO, T., TSENG, Y.-H. & KAHN, C. R. 2004b. Central role of suppressors of cytokine signaling proteins in hepatic steatosis, insulin resistance, and the metabolic syndrome in the mouse. *Proceedings of the National Academy of Sciences,* 101**,** 10422-10427.

UKAI, H., UKAI-TADENUMA, M., OGIU, T. & TSUJI, H. 2002. A new technique to prevent self-ligation of DNA. *Journal of Biotechnology, 97, 233-242.*

UNAIDS 2020, viewed 8 March 2021, <http://www.uniaids.org/en/resources/fact-sheet

UTECH, K., BERNEIS, K. 2005. Cachexia associated with AIDS. Semantic scolar

URNOV, F. D., MILLER, J. C., LEE, Y.-L., BEAUSEJOUR, C. M., ROCK, J. M., AUGUSTUS, S., JAMIESON, A. C., PORTEUS, M. H., GREGORY, P. D. & HOLMES, M. C. 2005. Highly efficient endogenous human gene correction using designed zinc-finger nucleases. *Nature,* 435**,** 646.

VAN OVERBEEK, M., CAPURSO, D., CARTER, M. M., THOMPSON, M. S., FRIAS, E., RUSS, C., REECE-HOYES, J. S., NYE, C., GRADIA, S. & VIDAL, B. 2016. DNA repair profiling reveals nonrandom outcomes at Cas9-mediated breaks. *Molecular Cell,* 63**,** 633-646.

VIGOUROUX, C., MAACHI, M., NGUYÊN, T.-H., COUSSIEU, C., GHARAKHANIAN, S., FUNAHASHI, T., MATSUZAWA, Y., SHIMOMURA, I., ROZENBAUM, W. & CAPEAU, J. 2003. Serum adipocytokines are related to lipodystrophy and metabolic disorders in HIV-infected men under antiretroviral therapy. *Aids,* 17**,** 1503-1511.

VINCENT, A. M., BROWNLEE, M. & RUSSELL, J. W. 2002. Oxidative stress and programmed cell death in diabetic neuropathy. *Annals of the New York Academy of Sciences,* 959**,** 368-383.

WOOD, A. J., LO, T.-W., ZEITLER, B., PICKLE, C. S., RALSTON, E. J., LEE, A. H., AMORA, R., MILLER, J. C., LEUNG, E. & MENG, X. 2011. Targeted genome editing across species using ZFNs and TALENs. *Science,* 333**,** 307-307.

XIAO, G., HARHAJ, E. W. & SUN, S.-C. 2001. NFκB-inducing kinase regulates the processing of NFκB2 p100. *Molecular Cell,* 7**,** 401-409.

YANG, Z., HULVER, M., MCMILLAN, R. P., CAI, L., KERSHAW, E. E., YU, L., XUE, B. & SHI, H. 2012. Regulation of insulin and leptin signaling by muscle suppressor of cytokine signaling 3 (SOCS3). *PloS One,* 7**,** e47493.

ZHANG, H. H., HALBLEIB, M., AHMAD, F., MANGANIELLO, V. C. & GREENBERG, A. S. 2002. Tumor necrosis factor-α stimulates lipolysis in differentiated human adipocytes through activation of extracellular signal-related kinase and elevation of intracellular cAMP. *Diabetes,* 51**,** 2929-2935.

ZHANG, J.-Z., BEHROOZ, A. & ISMAIL-BEIGI, F. 1999. Regulation of glucose transport by hypoxia. *American Journal of Kidney Diseases,* 34**,** 189-202.

ZIEGLER, D., HANEFELD, M., RUHNAU, K.-J., HASCHE, H., LOBISCH, M., SCHÜTTE, K., KERUM, G. & MALESSA, R. 1999. Treatment of symptomatic diabetic polyneuropathy with the antioxidant alpha-lipoic acid: a 7-month multicenter randomized controlled trial (ALADIN III Study). ALADIN III Study Group. Alpha-Lipoic Acid in Diabetic Neuropathy. *Diabetes Care,* 22**,** 1296-1301.

Appendices

Appendix A

UNIVERSITEIT VAN PRETORIA
UNIVERSITY OF PRETORIA
YUNIBESITHI YA PRETORIA

MSc Committee
School of Medicine
Faculty of Health Sciences

MSc
Committee
25 May 2018

Prof TS Pillay
Department of Chemical Pathology
Faculty of Health Sciences

Dear Prof,

Mr MC Mabugana, Student no 13077695

Please receive the following comments with reference to the MSc Committee submission of the abovementioned student:

Student name	Mr MC Mabugana	**Student number**	13077695
Name of study leader	Prof TS Pillay		
Department	Chemical Pathology		
Title of MSc	Analysis of the role of nuclear factor-kappa B in insulin resistance caused by antiretroviral drugs		
Date of first submission	April 2018		
May 2018	Thank you for submitting the revised protocol and required MSc form.		
Decision	This protocol has been provisionally approved. Please submit the revised protocol to ethics, and supply the MSc committee with proof of acceptance. The internal and external examiners can be nominated and submitted to the MSc Committee six months prior to submission of the dissertation. Please ensure that the CV of the examiners includes: supervision, examination and publication records.		

Yours sincerely

Prof Marleen Kock
Chair: MSc Committee

The Research Ethics Committee, Faculty Health Sciences, University of Pretoria complies with ICH-GCP guidelines and has US Federal wide Assurance.
- FWA 00002567, Approved dd 22 May 2002 and Expires 03/20/2022.
- IRB 0000 2235 IORG0001762 Approved dd 22/04/2014 and Expires 03/14/2020.

Pretoria 0001 South Africa
Tel +27 (0)12 319 2325
Fax +27 (0)12 323 0732

UNIVERSITEIT VAN PRETORIA
UNIVERSITY OF PRETORIA
YUNIBESITHI YA PRETORIA

Faculty of Health Sciences Research Ethics Committee

28/06/2018

Approval Certificate
New Application

Ethics Reference No: 346/2018

Title: Analysis of the role of nuclear factor-kappa B in insulin resistance caused by antiretroviral drugs.

Dear Mr Matamela. Mabugana

The **New Application** as supported by documents specified in your cover letter dated 5/06/2018 for your research received on the 5/06/2018, was approved by the Faculty of Health Sciences Research Ethics Committee on its quorate meeting of 27/06/2018.

Please note the following about your ethics approval:
- Ethics Approval is valid for 2 years
- Please remember to use your protocol number (**346/2018**) on any documents or correspondence with the Research Ethics Committee regarding your research.
- Please note that the Research Ethics Committee may ask further questions, seek additional information, require further modification, or monitor the conduct of your research.

Ethics approval is subject to the following:
- The ethics approval is conditional on the receipt of **6 monthly written Progress Reports**, and
- The ethics approval is conditional on the research being conducted as stipulated by the details of all documents submitted to the Committee. In the event that a further need arises to change who the investigators are, the methods or any other aspect, such changes must be submitted as an Amendment for approval by the Committee.

We wish you the best with your research.

Yours sincerely

Dr R Sommers; MBChB; MMed (Int); MPharMed,PhD
Deputy Chairperson of the Faculty of Health Sciences Research Ethics Committee, University of Pretoria

The Faculty of Health Sciences Research Ethics Committee complies with the SA National Act 61 of 2003 as it pertains to health research and the United States Code of Federal Regulations Title 45 and 46. This committee abides by the ethical norms and principles for research, established by the Declaration of Helsinki, the South African Medical Research Council Guidelines as well as the Guidelines for Ethical Research: Principles Structures and Processes, Second Edition 2015 (Department of Health).

☎ 012 356 3084 deepeka.behari@up.ac.za / fhsethics@up.ac.za http://www.up.ac.za/healthethics
✉ Private Bag X323, Arcadia, 0007 - Tswelopele Building, Level 4, Room 60 / 61, 31 Bophelo Road, Gezina, Pretoria

Renewal certificate. Matamela Mabugana. 2020.pdf

Appendix B

1. Ham's F12 mixture culture medium

Reagent	Volume/ mass	Final concentration
Ham's F12 medium	437 ml	
Foetal calf serum (FCS)	50 ml	10 %
200 mM Glutamine	5 ml	2 mM
100 x Antibiotic/antimycotic solution	5 ml	1 %
Gentamicin	2.5 ml	0.5 %
*G418	0.5 ml	400 µg/ml
Total volume	500 ml	

* 0.4 g G418-sulphate powder was dissolved in 1 ml dH_2O and filtered using a 0.2 µM syringe filter.

2. 10 X Lysis buffer stock solution

Reagent	Volume/mass	Final concentration
4-(2-hydroxyethyl)-1-piperazineethanesulfonic acid (HEPES), pH 7.5	445 ml	50 mM
Phenoxylpolyethoxyethanol (NP40)	5 ml	1 %
Glycerol	50 ml	10 %
Sodium chloride (NaCl)	1.461 g	50 mM
Total volume	**500 ml**	

2. 1 x Lysis buffer solution

The lysis buffer was prepared with 1 tablet of protease inhibitor and 1 tablet of phosphatase inhibitor in 10 ml of 10 x lysis buffer stock solution

3. Freezing solution for CHO-IR cells

Reagents	Volume/mass	Final concentration
Dimethyl sulphoxide (DMSO)	5 ml	10 %
FCS	45 ml	
Total volume	**50**	

4. Phosphate buffered saline (PBS)

1 tablet of PBS was dissolved in 100 ml dH_2O and the mixture was filtered sterile with a syringe filter

5. Calculation of cell number

CHO-IR cells were counted using a haemocytometer to determine the total number of cells in the original flask. Then, 10 µl cell medium solution was loaded into the haemocytometer. The number of cells in 5 of 10 0.1 mm^3 blocks was counted as follows:

Cells cm^3 = Number of cells counted / Number of squares counted x conversion factor (1000)

100 000 cells per well of each 6-well plate was required to achieve 70-85 % confluence on day 2/3.

6. 10 % Ammonium persulphate (APS)

0.1 g APS was dissolved in 1 ml dH2O

7. 10 % SDS

5 g SDS was dissolved in 50 ml dH2O

8. 4 % stacking gel

Reagents	Volume	Final concentration
0.5 M Tris-HCl, pH 6.8	1.260 ml	0.126 M
30 % Acrylamide/bis (19:1)	0.660 ml	4 %
dH2O	3.000 ml	
10 % SDS	0.500 ml	0.1 %
10 % APS	0.250 ml	0.05 %
TEMED	0.005 ml	0.1 %
Total volume	5.675 ml	

9. 7.5 % resolving gel

Reagents	Volume (ml)	Final concentration
1.5 M Tris-HCl, pH 8.8	2.500 ml	0.375 M
30 % Acrylamide/bis (19:1)	2.500 ml	7.5 %
dH2O	4.850 ml	
10 % SDS	0.100 ml	0.1 %
10 % APS	0.050 ml	0.05 %
TEMED	0.005 ml	0.05 %
Total volume	10.005 ml	

10. 10 X Running buffer

Reagents	Volume/mass	Final concentration
Tris base	14.41 g	0.025 M
Glycine	3 g	0.192 M
SDS	1 g	0.1 %
dH2O	1 l	
Total volume	1 l	

1 x Running buffer
100 ml 10 x stock solution was added to 900 ml deionised water.

11. 10 X Transfer buffer

Reagents	Volume/mass	Final concentration
Tris base	30.28 g	0.025 M
glycine	144.13g	0.192 M
dH2O	800 ml	
Total volume	800 l	

1 x Transfer buffer
80 ml 10 x stock solution was added to 720 ml deionised water and 200 ml methanol.

12. Tris-buffered saline + 0.1 % Tween 20 (TBST), pH 7.4

Reagents	Volume/mass	Final concentration
Tris-HCl	6.8 g	0.05 M
Tris base	0.82 g	
NaCl	8.77 g	0.150 M
Tween 20	5 ml	0.1 %
dH2O	1 l	
Total volume	1 l	

14. 0.1 % Ponceau S solution

0.1 g Ponceau was dissolved in 100 ml of 5 % acetic acid.

15. 3 % BSA

1.5 g BSA was dissolved in 50 ml TBST.

16. 5 % Milk solution

2.5 g skimmed milk powder (Spar, South Africa) was dissolved in 50 ml TBST.

17. Transformation and storage solution (TSS)

Reagants	Volume/mass	Final concentration
PEG 8000	20 g	20 %
DMSO	10 ml	10 %
MgCl	2.03 g	10 Mm
LB medium	100 ml	

Autoclave

18. 10 X Tris-Borate EDTA

Reagent	Volume/mass	Final concentration
Tris base	108 g	1.3 M
Boric acid	55 g	450mM
0.5 M EDTA	40 ml	25 mM
ddH_2O	900 ml	

For 1 X TBE, 100 ml of 10 X TBE was diluted in 900 ml ultrapure water

19. 10 X Tris-acetate EDTA

Reagent	Volume/mass	Final concentration
Tris base	48.5 g	4.0 M
Glacial acetic acid	11.4 ml	
0.5 M EDTA	20 ml	0.1 mM
ddH_2O	900 ml	

For 1 X TAE, 100 ml of 10 X TAE was diluted in 900 ml ultrapure water

20. 2 X HEPES bufferd saline (HBS), pH , 7.2*

Reagent	Volume/ Mass	Final concentration
NaCl	8.0 g	280 mM
HEPES	5.0 g	50 mM
ddH_2O	500 ml	
$Na_2HPO_4.7H_2O$	0.188 g	1.5 mM
KCl	0.37 g	10 mM
Dextrose	1.0 g	12 mM

*Filter strerilised

21. 10 X LB broth

20.6 g of LB broth was mixed with 1L MilliQ water, autoclaved.

22. 10 X LB Agar

35 g of LB powder was mixed with 1l Milliq water

23. 8 % TBE electrophoresis gel

Reagents	Volume	Final cocentration
Acrylamid:bis-acrylamide (29:1)	7 ml	8 %
10 X TBE	3.5 ml	1 %
ddH_2O	23.5 ml	
APS	175 µl	0.1 %
TEMED	35 µl	0.1 %
10 % SDS	1	0.1 %

24. 0.5 µg/ml Ethidium Bromide

1 µl of 10 µg/ml ethidium bromide solution was added in 20 ml of ddH_2O